DOI: 10.24850/j-tyca-14-02-02

Articles

# Space evolution of turbulent structures over a flexible vegetation area

# Evolución espacial de las estructuras turbulentas sobre una zona de vegetación flexible

Edwin Jonathan Pastrana[1], ORCID: https://orcid.org/0000-0002-8403-3701

Ariosto Aguilar-Chávez[2], ORCID: https://orcid.org/0000-0002-2884-5908

Ángel Mendoza-González[3], ORCID: https://orcid.org/0000-0002-2883-2330

[1]National Autonomous University of Mexico, Mexico City, Mexico, edwin.pastrana@posgrado.imta.edu.mx

[2]Mexican Institute of Water Technology, Jiutepec, Mexico, aaguilar@tlaloc.imta.mx

[3]National Autonomous University of Mexico, Mexico City, Mexico, angelmg@comunidad.unam.mx

Corresponding author: Edwin Jonathan Pastrana, edwin.pastrana@posgrado.imta.edu.mx

**Abstract**

In a natural or artificial channel, the presence of vegetation at the bottom and on the wall is usual. The effects produced by the presence of this is an alteration of the flow field. The magnitude of the changes in the flow field depends on the extension, height, density, and flexibility of the vegetation. To analyze the turbulent structures in detail in this work, an experimental study was carried out in a laboratory, in a rectangular channel with a section of submerged, flexible, and artificial vegetation. The measurement region was located upstream of the vegetation zone until the end of it, in addition, the asymmetry that the presence of the channel wall can induce was determined. The measurements were performed with an Acoustic Doppler Velocimeter (ADV) instrument. The results allow to identify the development of the mixing layer from the average velocity patterns and the Reynolds stress. In the case of the average velocity profiles over the vegetation layer, it was possible to identify an inflection point where Kelvin-Helmholtz instabilities type were identified. In order to analyze the processes in the mixing layer, a phenomenological model is proposed based on the analysis of the curvature of the averaged velocities. In addition, the contribution to the moment transport rate by the identified turbulent structures were determined with a quadrant analysis of fluctuating velocities.

**Keywords**: Flexible vegetation, phenomenological model, ADV, mixing layer, turbulent structures.

Tecnología y Ciencias del Agua

OPEN ACCESS

Check for updates

**Resumen**

En un cauce natural o artificial es usual la presencia de vegetación en el fondo y en la pared. Los efectos que produce la presencia de ésta es una alteración en el campo de flujo. La magnitud de las alteraciones en el campo del flujo depende de la extensión, altura, densidad y flexibilidad de la vegetación. Para analizar a detalle las estructuras turbulentas, en este trabajo se realizó un estudio experimental en laboratorio en un canal de sección rectangular con un tramo de vegetación sumergida, flexible y artificial. La región de medición se ubicó aguas arriba de la zona de vegetación hasta el final de esta misma, además se determinó la asimetría que puede inducir la presencia de la pared del canal. Las mediciones se realizaron con equipo de velocimetría acústica de efecto Doppler (ADV). Los resultados obtenidos identifican el desarrollo de la capa de mezcla a partir de los patrones de velocidad media y los esfuerzos de Reynolds. En el caso de los perfiles de velocidad media sobre la capa de vegetación fue posible identificar un punto de inflexión donde se identificaron inestabilidades tipo Kelvin-Helmholtz. Con el fin de analizar los procesos en la capa de mezcla se propone un modelo fenomenológico basado en el análisis de la curvatura de las velocidades promediadas. Además, se determinó la aportación en el transporte de momento de las estructuras turbulentas con un análisis de cuadrantes con las velocidades fluctuantes.

**Palabras clave**: vegetación flexible, modelo fenomenológico, ADV, capa de mezcla, estructuras turbulentas.

Received: 11/11/2020
Accepted: 20/09/2021

# Introduction

In an artificial channel the interaction of the flow with the vegetation produces a wake zone and generates regions of turbulence production that alter the patterns of average flow, with a remarkably high three-dimensional rate.

In the case of a natural channel the presence of submerged vegetation is normal, but changes in its morphology are related to its presence and interfere depending on its height, density and flexibility. Vegetation generates changes in turbulent structures vertically and transversely, as well as important secondary flows. To evaluate the magnitude of these changes it is advisable to estimate patterns of average flows and Reynolds stresses, as a low frequency characterization condition, but also to evaluate the fluctuating velocities statistically.

This part of the document describes the conditions of submergence, bending and density of vegetation. The condition of submergence,

according to Palmer (1945) establishes it as the relationship between the height of the vegetation with respect to the water depth of the channel. The internal composition of this is very important, since it influences in a very specific way in the modification of the bottom of the channel. In addition, an important parameter to consider, should be the relationship between the bending response of vegetation elements in relation to the kinetics of the flow field.

The flexion of vegetation ($\mathcal{J}$) is the dynamic response of the structure of the stems of vegetation to the action of the main velocity of flow (Okamoto & Nezu, 2010; Ghani *et al.,* 2013; Jeon, 2015). This is a function of the main velocity and can be classified according to the experimental results obtained by Carollo *et al.,* (2005), and Okamoto & Nezu (2009), this classification is listed below:

I. Rigid. The vegetation is maintained in its vertical position and does not present oscillations in the top.
II. Smooth oscillation. The vegetation has a smooth deformation and has an unorganized smooth oscillation.
III. Monami. The vegetation has a significant deformation, and a coherent and harmonic oscillatory motion is observed.
IV. Prone. The vegetation has a despondency of all its elements and the oscillations are small with high frequency.

In addition to the bending behavior, vegetation can be classified with respect to its location and distribution which can be on the wall or bottom of the channel, exclusively or in both places. It's also important

to establish the density of vegetation, which can induce different behaviors for the same type of relationship between velocity and bending (Poggi *et al.*, 2004; Nezu & Sanjou, 2008).

The relationship between vegetation height and water depth, defined by Nepf & Vivoni (2000) are classified into three types:

I. Low flows, the flow passing through the stems and foliage are deformed.
II. Intermediate flows, have a complete submergence of vegetation, but it affects the behavior of the flow field.
III. High flows, the flow field is not affected by the presence of vegetation, for this condition the vegetation is considered as a uniform bottom roughness.

The study of intermediate flows has become an important topic to analyze due the effects that are generated in the mean and turbulent flow, since they modify the profiles of average velocity generating coherent turbulent structures near the top of the vegetation and these vortices are mainly large-scale, generating an exchange zone of mass and momentum, between the vegetation top and outer zone, that is, on the vegetation, a condition similar to a boundary layer. In engineering practice submerged vegetation is analyzed as a condition of uniform resistance, similar to a high flow. Then, to evaluate its effect, the usual concept of the resistance of the flow by effect of the submerged vegetation and its effects on the roughness parameters is applied,

obtaining general values of Manning's roughness coefficient as a function of the submergence ratio (Järvelä, 2004; Wilson, 2007).

In this work we will carry out a more localized study of the effects of submerged vegetation, considering that the development of the flow field on the top of the vegetation is similar to the condition of two flow fields at different velocities and with a layer of interaction between these and that produces small perturbations, which induce an instability of the flow of the Kelvin-Helmoholtz (KH) type, so above large-scale vortices are generated, as Finnigan (2000) demonstrate. To analyze in greater detail the generation of turbulent structures in principle it can be said that have a boundary layer and this develops longitudinally, but Ghisalberti & Nepf (2002) demonstrate that flows on submerged vegetation can be analyzed as a mixing layer, rather than as a boundary layer. The velocity profile of a mixing layer approximates the shape of a hyperbolic tangent profile (Ho & Huerre, 1984), as shown in Figure 1.

Tecnología y Ciencias del Agua
OPEN ACCESS
Check for updates

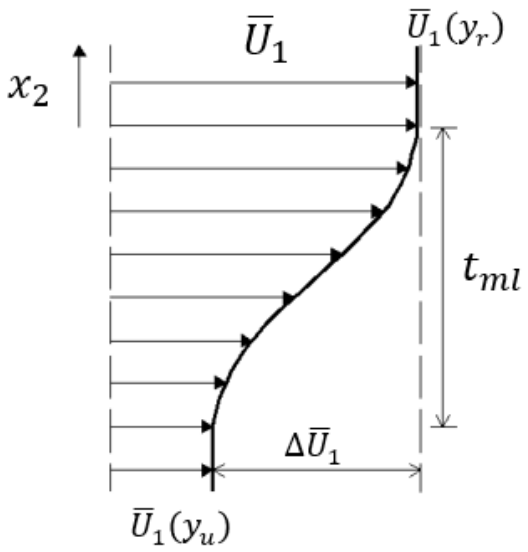


**Figure 1**. Velocity type profile in a blend layer (Ghisalberti & Nepf, 2002).

According to Poggi *et al.* (2004) in the vegetation zone three regions can be identified, according to the size of the vortices, as shown in Figure 2. The first region is mainly dominated by small-scale vortices (von Kármán vortices). The second region, which is near the top of vegetation is dominated by Kelvin-Helmholtz vortices generated by instability at the inflection point. The third region is similar to a boundary layer-like development zone.

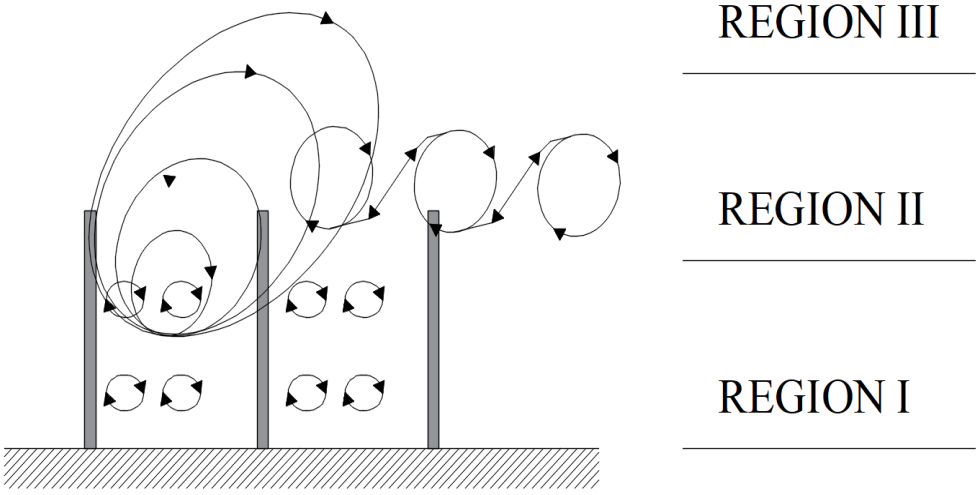


**Figure 2**. Three vortices scales in a channel with submerged vegetation (Poggi *et al*., 2004).

Sukhodolov & Sukhdolova (2006) performed field measurements to verify the applicability of the analogy of the mixing layer in a natural channel, on a patch of *Sagittaria sagittifolia* implanted with a certain arrangement varying their density. The results confirm the effectiveness of the mixing layer analogy. Sukhodolov & Sukhdolova (2006), and Maltese *et al.* (2007) focused on the spatial pattern of the turbulent structure that develops over submerged vegetation. In addition, they applied quadrant analysis, revealing that the dominant structure is the expulsion on the vegetation top.

Ghisalberti & Nepf (2002) revealed that flows with submerged vegetation can be modeled ¿ as a mixing layer, rather than a boundary

layer zone, because the velocity profiles that occur in a channel with submerged vegetation approximate a hyperbolic tangent profile, see Figure 1. In addition, from the average velocity profiles they identify an inflection point, which implies that the flow is susceptible to Kelvin-Helmholtz instabilities. Nikora *et al.* (2008) examine the effect of submerged vegetation on hydraulic resistance in a variety of vegetation patch patterns. Okamoto *et al* (2012) performed continuous inkjet experiments to evaluate the structure of mass transport in an open channel flow with rigid vegetation models, and a rigid strip configuration varying density. Obtaining the effects of coherent vortices on vertical turbulent diffusion. Okamoto & Nezu (2013) examined the transition from a boundary layer upstream the vegetation patch to a mixing layer type flow developed over the vegetation and developed a phenomenological model for the development process in the flow with submerged vegetation. In these experiments they used the PIV (Particle Image Velocimetry) technique, and the vegetation elements were composed of rigid strips.

As mentioned above, the characteristics of mean flow and turbulence in open channel flows with submerged vegetation have received a lot of attention. However, detailed information on the evolution of the mixing layer and the coherent turbulent structures generated by the presence of vegetation is not yet available. For this reason, the present study considers the effect of a patch of flexible vegetation of finite length and an intermediate flow to identify turbulent structures, as well

as their longitudinal and transverse evolution from a phenomenological model. The analysis zone starts upstream of the patch to the patch boundary, but cross-sectional measurements were made and vertically the area below the vegetation top to the outer flow was considered.

## Materials and methods

The experimental station is a channel with fixed slope $S_0$ of rectangular section, with a length of $10\ m$, a width of $0.60\ m$ and with a height of $0.60\ m$. The walls of the channel are made of glass and steel bottom. The representation of the vegetation elements is of a flexible plastic material. The hydraulic conditions of the experimental study are shown in Table 1.

**Table 1**. Hydraulic conditions. Where $\boldsymbol{Q}$ is the flow rate, $\boldsymbol{U = Q/A}$ is the average velocity of the flow, $\boldsymbol{S_0}$ is the slope of the channel, $\boldsymbol{Re = UR_h/\nu}$ is the Reynolds number, $\boldsymbol{Fr = U/\sqrt{gR_h}}$ is the Froude number, $\boldsymbol{R_h = A/P}$ is the hydraulic radius, $\boldsymbol{A}$ is the area of the cross-section, $\boldsymbol{P}$ is the perimeter of the cross-section, $\boldsymbol{\nu}$ is the kinematic viscosity and $\boldsymbol{g}$ is the acceleration of gravity.

| $\boldsymbol{h}$ (cm) | $\boldsymbol{h_p}$ (cm) | $\boldsymbol{h/h_p}$ | $\boldsymbol{Q}$ ($\mathbf{l\,s^{-1}}$) | $\boldsymbol{U}$ ($\mathbf{cm\,s^{-1}}$) | $\boldsymbol{S_o}$ | $\boldsymbol{Re}$ | $\boldsymbol{Fr}$ |
|---|---|---|---|---|---|---|---|
| 33 | 11 | 3 | 41.20 | 20 | 0.005 | 32698 | 0.11 |

The reference system for sampling from the experimental station is shown in Figure 3. Where the coordinate system is the triad of values of $x_i$, for $i = 1,2,3$, and is named as longitudinal, vertical and transverse coordinate respectively. The domain of the measuring space in meters is $\Omega(x_i) \in [-0.5, 3.7] \times [0.0, 0.33] \times [0.0, 0.3]$.

Tecnología y Ciencias del Agua
OPEN ACCESS
Check for updates

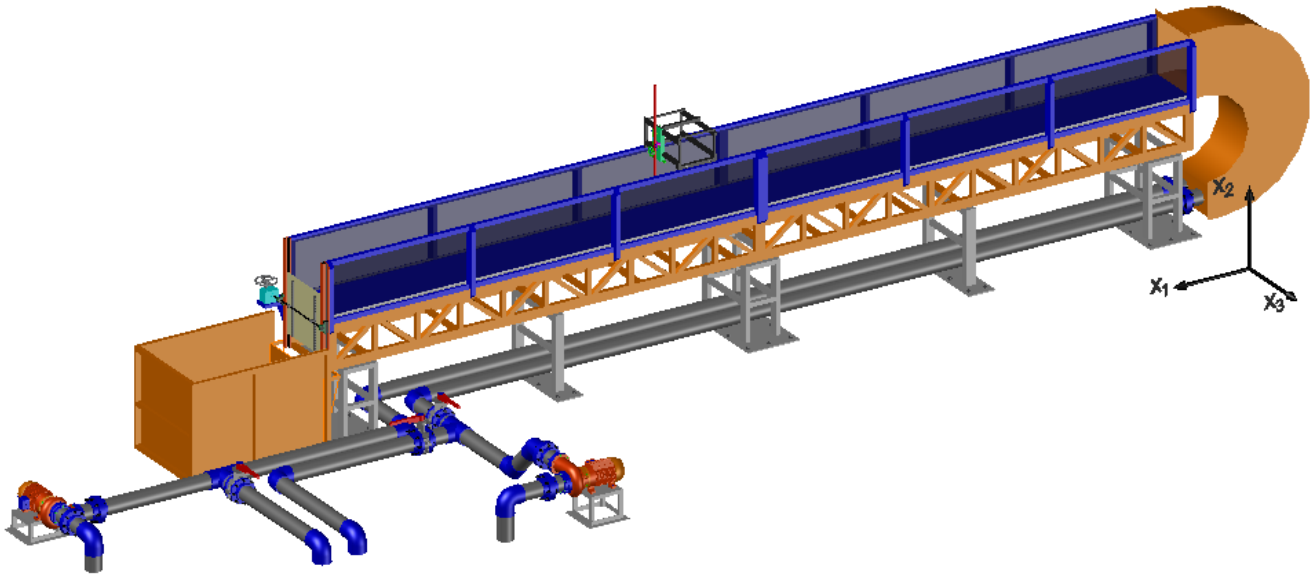


**Figure 3**. Experimental station.

For sampling of the instantaneous velocities in the three components $(u_i)$, an Acoustic Doppler velocimetry (ADV) device was used at a sampling frequency rate of $100\,Hz$ during a period of $T = 60\,s$. The ADV device is of the Nortek® or also called Vectrino Profiler™ (Vectrino II). For the processing of the experimental data, we considered the Reynolds decomposition model $u_i \equiv U_i + u_i'$, considering the temporal averaged velocities in each component as $U_i$ and the fluctuating velocities as $u_i'$.

The vegetation configuration is a patch with a length of $3.70\,m$ and the arrangement of flexible elements is linear, with a separation between elements in longitudinal direction is $l_{x_1} = 0.025\,m$, and in transverse

direction is $l_{x_3} = 0.025\,m$, as shown in Figure 4 and Figure 5, respectively. The start of the vegetation patch is considered in $x_1 = 0$.

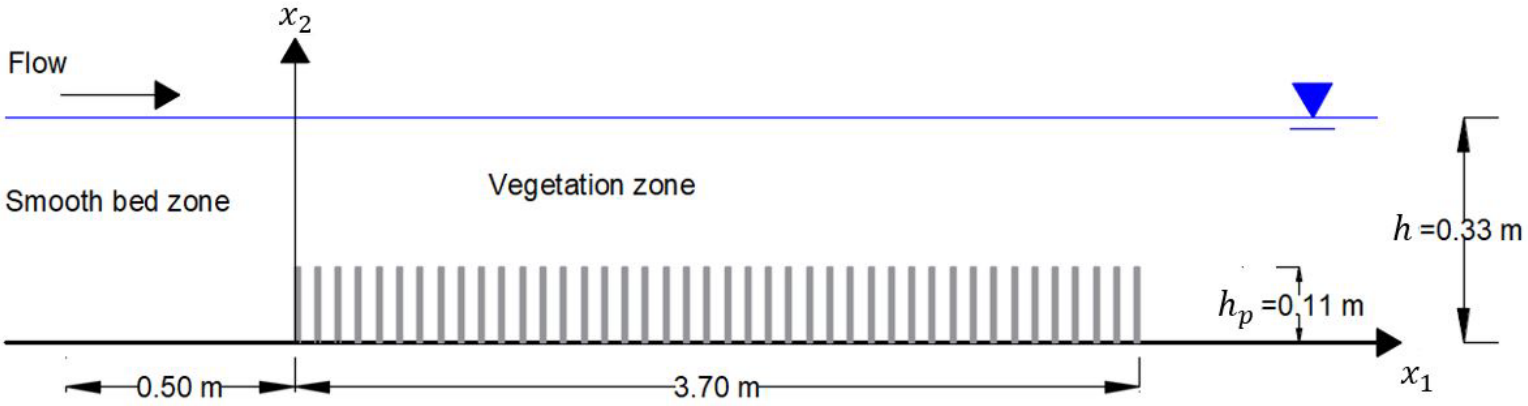


**Figure 4**. Vegetation zone.

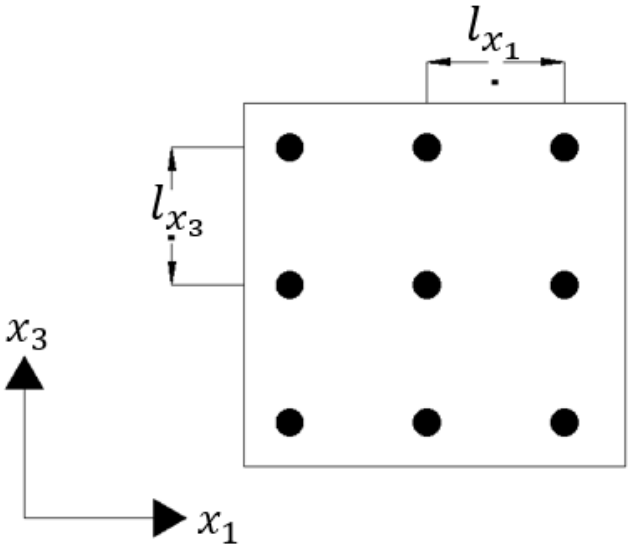


**Figure 5**. Patron of vegetation elements.

The sampling points were from the center of the channel to the right bank in five sections, indicated by the $A, B, C, D, E$ letters, see Figure 6 and longitudinally $43$ points were analyzed and $19$ vertically, see Figure 7a. The measurement points in the vertical are shown in Figure 7b.

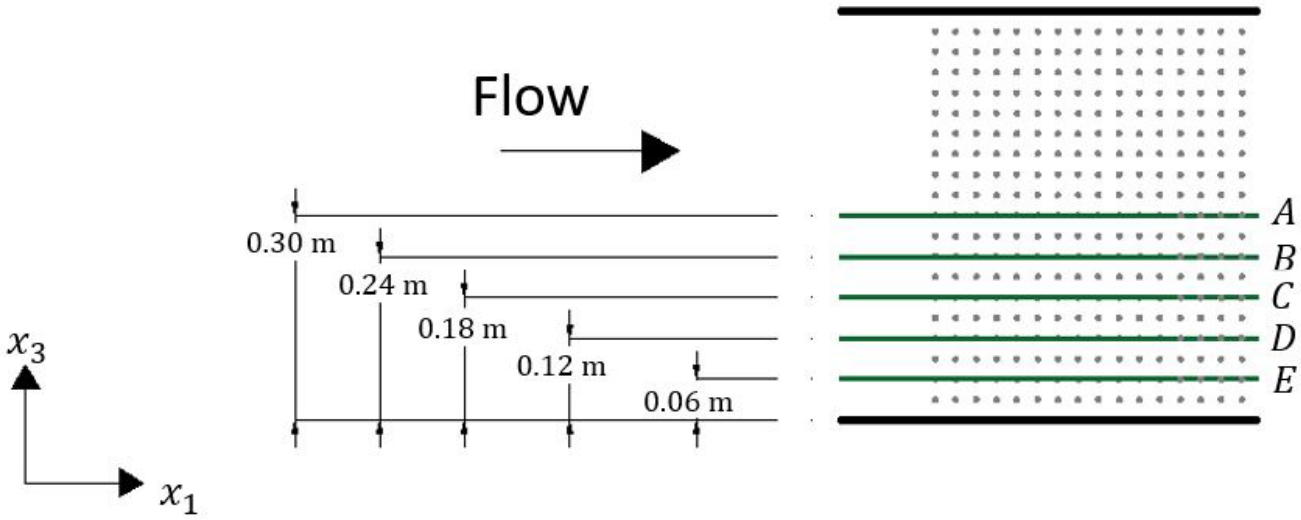


**Figure 6**. Measurements in the transverse direction.

Tecnología y Ciencias del Agua
OPEN ACCESS
Check for updates

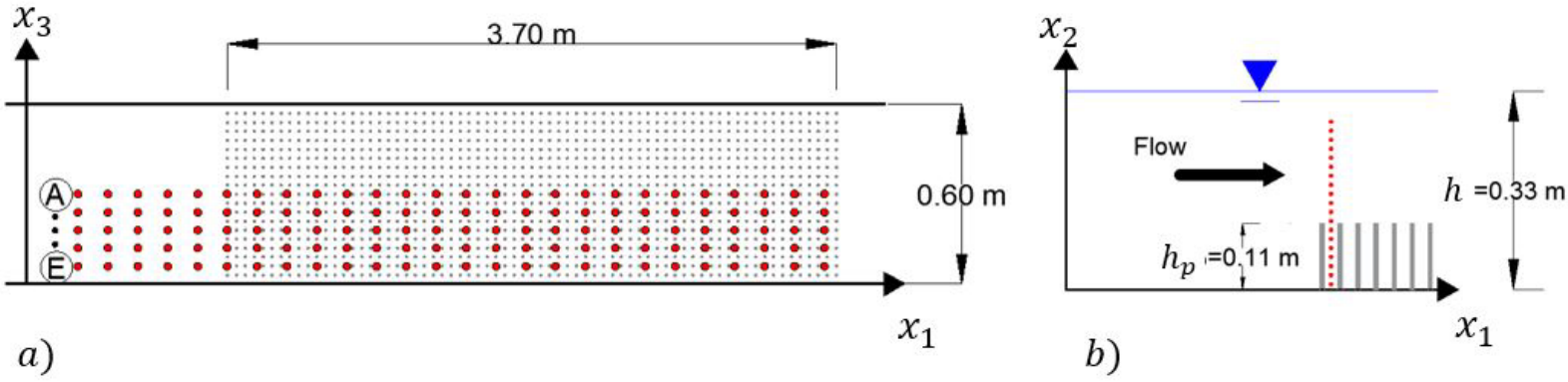


**Figure 7**. Measurement points with the ADV equipment, with a total of $\mathbf{4085}$ points. a) Sampling points in the plane $(\boldsymbol{x_1}, \boldsymbol{x_3})$ with a separation of $\mathbf{0.10}\,\boldsymbol{m}$ in the direction $\boldsymbol{x_1}$ and $\mathbf{0.06}\,\boldsymbol{m}$ in the direction $\boldsymbol{x_3}$; b) Sampling points in the plane $(\boldsymbol{x_1}, \boldsymbol{x_2})$ with a separation of $\mathbf{0.015}\,\boldsymbol{m}$ in the direction $\boldsymbol{x_2}$. In the vegetation zone there are $\mathbf{7}$ points inside and $\mathbf{12}$ above the vegetation.

According to Vargas-Luna *et al.* (2015), the actual vegetation can be simulated with cylindrical bars. With this, it was proposed to use cylindrical bars to simulate vegetation with the following physical characteristics: a height of $h_p = 0.11\,m$ and a diameter of $\emptyset = 7.3\,mm$, the material of the vegetation elements is silicone.

For the characterization of the vegetation were used the parameters of vegetation density, $\lambda_f$, flexural rigidity, $\mathcal{J}$, and the ratio of submergence, $h/h_p$. The dimensionless vegetation density, $\lambda_f$, was determined with the expression proposed by Okamoto & Nezu (2013):

$$\lambda_f = \frac{\sum_i^{n_v} A_{f_i} h_p}{A_b h_p} \quad (1)$$

Where $A_f$ is the total frontal area of the vegetation elements, $A_b$ is the area occupied by the vegetation. In the case of flexural rigidity, $\mathcal{J}$, of vegetation elements, the equation proposed by Wilson *et al* (2003), was used, and is:

$$\mathcal{J} = EI = \frac{F}{\delta_{x_1}} \frac{L^3}{3} \quad (2)$$

Where $E$ is the modulus of elasticity, $I$ the second moment of the area (also called the moment of inertia). On the right side of the expression, we have that $F$ is the relationship between the force, $\delta_{x_1}$it is the deflection of the element, $L$ it is the length of the vegetation element (Figure 8). Then, we get a value of $\mathcal{J} = 3.42x10^{-3}\, Nm^2$ and a value $\lambda_f = 1.37$.

Tecnología y Ciencias del Agua
OPEN ACCESS
Check for updates

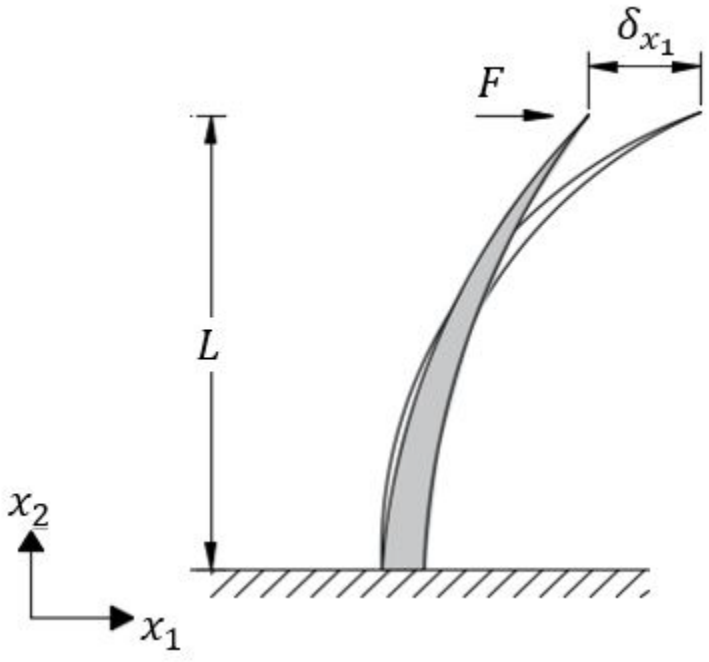


**Figure 8**. Diagram of the vegetation element with deflection.

For this study we simulated a type of real vegetation called *Lespedeza sericea* with a length of $h_p = 10 - 20\,cm$ and with a $\mathcal{J} = 5x10^{-6}$ $1x10^{-3}\,Nm^2$ (Kouwen & Li, 1980; Nepf & Vivoni, 2000). The parameters used in this experiment, such as, the submergence ratio, the density, the flexural rigidity and the pattern of the vegetation elements, was based on various laboratory experiments carried out by various authors (Palmer, 1945; Wilson *et al*., 2003; Nezu & Sanjou, 2008; Okamoto & Nezu, 2013). Linear and stepped patterns are the most used in the laboratory, because they have a better representation of the effect of vegetation in a channel with intermediate flow (Vargas-Luna *et al*., 2015).

Tecnología y Ciencias del Agua

OPEN ACCESS

Check for updates

# Results

According to the above, the flow condition being analyzed is an intermediate flow. In addition, for a better understanding of the results we considered a dimensionless space of the sample domain $\Theta(\xi_i = x_i/h_p) \in [-4.54, 33.63] \times [0.0, 3.0] \times [0.0, 2.72]$, the top of the vegetation is held for $\xi_2 = 1$, and the start of the vegetation for $\xi_1 = 0$. For the cross-sectional sections shown in Table 2.

**Table 2**. Values of $\boldsymbol{\xi_3}$ for the measurement points in the transverse direction.

| **Section** | $\boldsymbol{A}$ | $\boldsymbol{B}$ | $\boldsymbol{C}$ | $\boldsymbol{D}$ | $\boldsymbol{E}$ |
|---|---|---|---|---|---|
| $\boldsymbol{\xi_3 = x_3/h_p}$ | 2.72 | 2.18 | 1.63 | 1.09 | 0.54 |

Tecnología y Ciencias del Agua

OPEN ACCESS

Check for updates

## Mean flow characteristics

Of the measurements obtained, the fields of mean flows were first analyzed. Figure 9 shows the temporal mean velocity contours in the main direction $U_1$. The mean velocity at the sampling points $(\xi_i)$ was determined with the following expression.

$$U_i(\xi_i) = \frac{1}{T}\int_0^{\eta=t} u_i(\xi_i, \eta)d\eta \qquad (3)$$

Tecnología y Ciencias del Agua

OPEN ACCESS

Check for updates

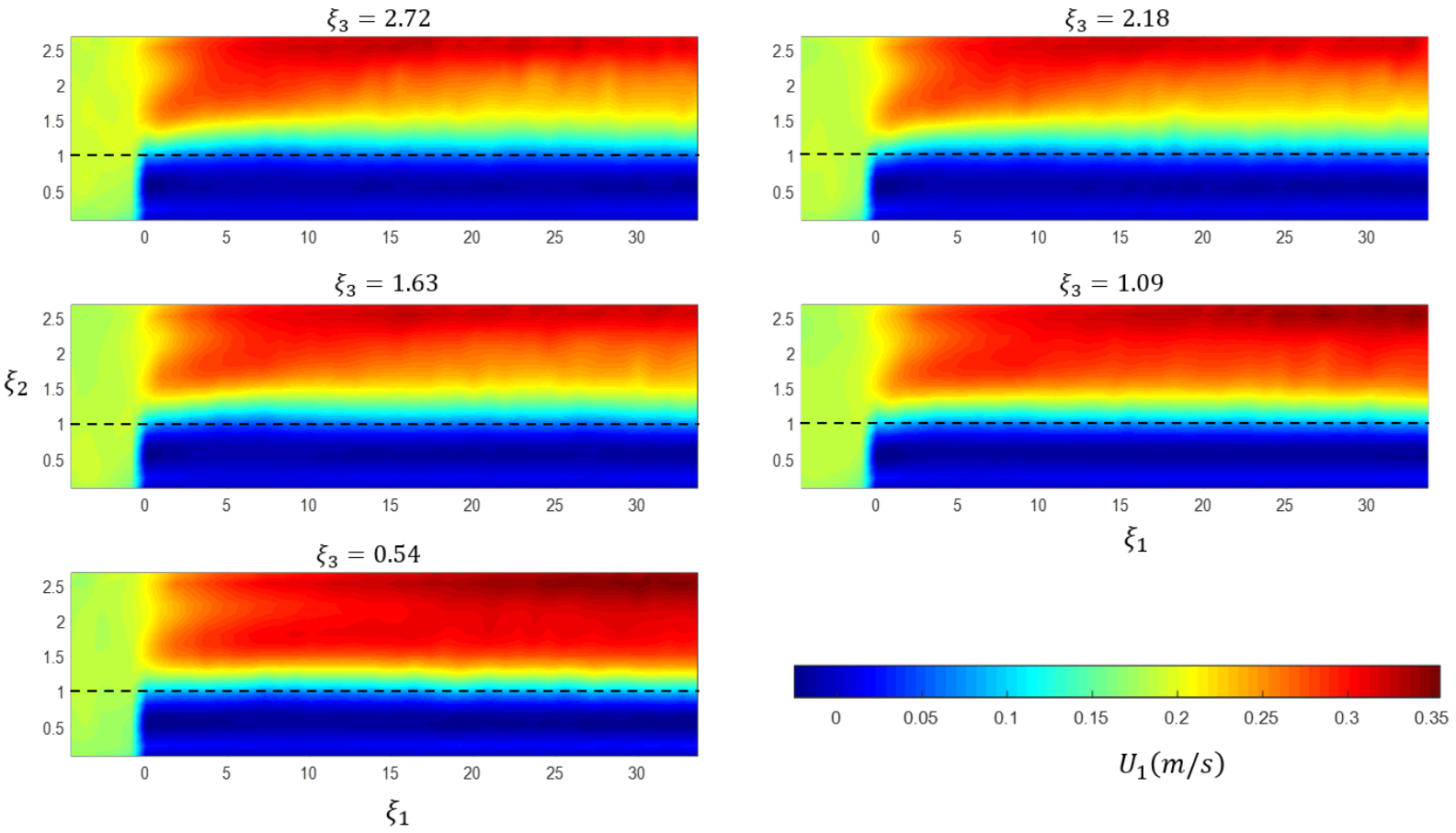


**Figure 9**. Contours of mean velocity in the main direction $\boldsymbol{U_1}$. Where the dashed line represents the top of the vegetation $\boldsymbol{\xi_2 = 1}$.

Due to the presence of the vegetation, a deceleration of the main velocity is observed near the vegetation top $\xi_2 \approx 1$, which is compensated by an increase in this in the outer zone. This distortion of the flow field causes an inflection point right in the vegetation top $\xi_2 = 1$, the above generates a Kelvin-Helmholtz instability and therefore vortices of different

scales are presented, this observation resembles results presented by Nepf & Vivoni (2000).

In addition, Figure 10 shows the mean velocity profiles for all cross sections, observing a hyperbolic profile. These flow field characteristics are similar to those presented in terrestrial vegetation, presented by Finnigan (2000). The instability is maintained in the transverse direction, but the thickness of the mixing layer decreases due to the presence of the wall.

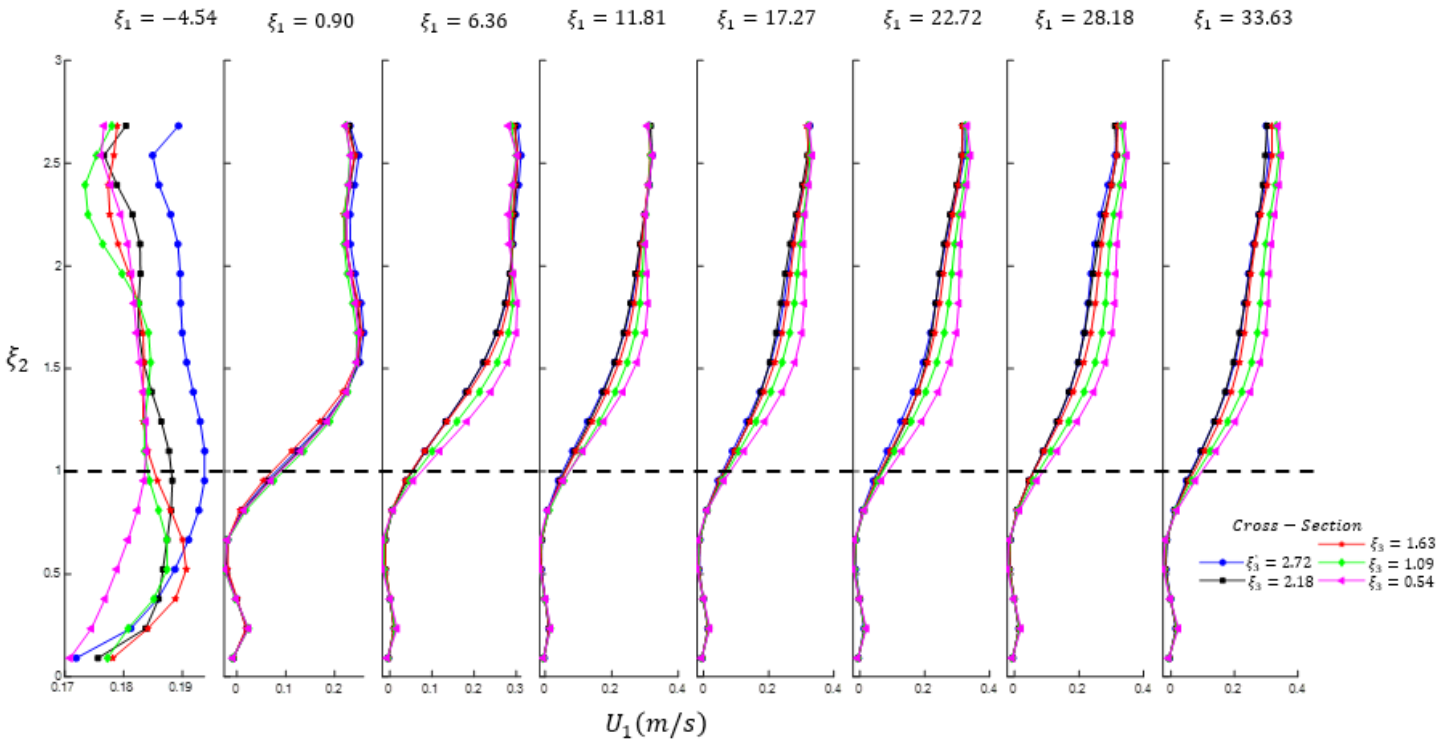


**Figure 10**. Mean velocity profiles in the main direction, $U_1$. Where the dashed line indicates the top of the vegetation.

The mean velocity profile in $\xi_1 = -4.54$, see Figure 10, in the zone near the free surface ($\xi_2 \geq 2.5$), an acceleration of the flow is observed by the backwater effect caused by the vegetation.

## Reynolds stress

Analyzing Reynolds stress $-\overline{u_1' u_2'}$ of the experiments (Figure 11), the development of the mixing layer can be observed, which is very representative for the central area ($\xi_3 = 2.72$), but this is decreasing as the influence of the walls is had, $\xi_3 < 2.72$.

Tecnología y Ciencias del Agua

OPEN ACCESS

Check for updates

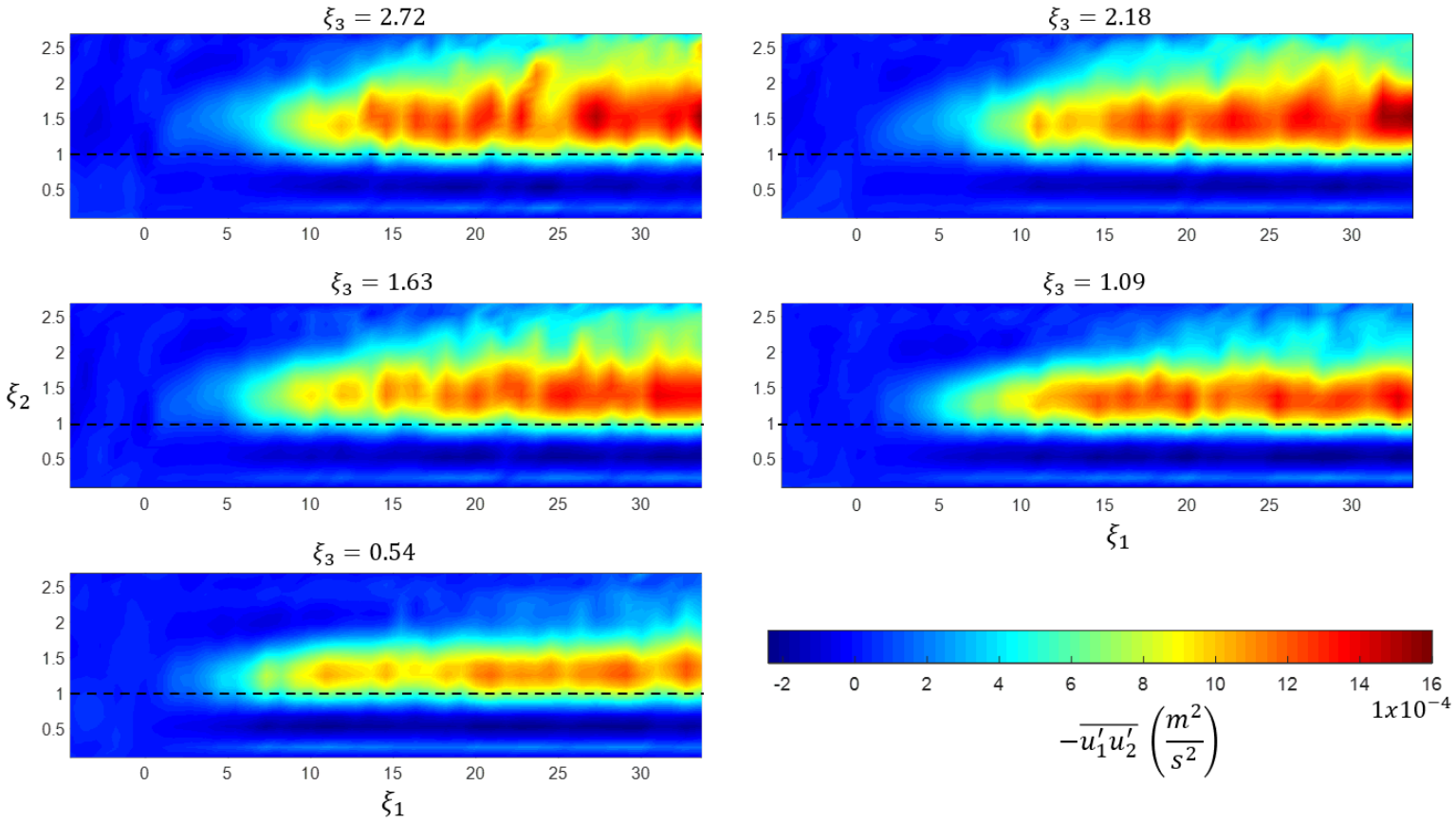


**Figure 11**. Reynolds stress contours $-\overline{u_1'u_2'}$ . Where the dashed line represents the top of the vegetation $\xi_2 = 1$.

Nepf & Vivoni (2000), Nezu & Sanjou (2008) define the size of the mixing layer from the Reynolds stress profiles $-\overline{u_1'u_2'}$, where the upper and lower limit are defined by the $10\,\%$ of the maximum stress $\left|-\overline{u_1'u_2'}\right|_{max}$, that is, as shown in the following expression:

$$y_u, y_r = \frac{1}{\left|-\overline{u_1' u_2'}\right|_{max}} \frac{\partial\left(\left|-\overline{u_1' u_2'}\right|_{max}\right)}{\partial x_2} \quad (4)$$

Where $y_r$ is the upper limit and $y_u$ is the lower limit of the mixing layer. The upper and lower limits of the mixing layer for $\xi_3 = 2.72$ and $\xi_3 = 0.54$ are shown in Reynolds stress profiles, according to the profile of Reynolds stresses for the longitudinal position, and in the cross section $\xi_1 = 33.63$you have a mixture layer thickness of and $\xi_3 = 2.72$for $t_{ml_A} \approx 0.19\, m$of $\xi = 0.54$. $t_{ml_E} \approx 0.15\, m$ (Figure 12). With this it is observed that at the center of the channel you have a larger mixture layer size than you have glued to the wall.

Tecnología y Ciencias del Agua

OPEN ACCESS

Check for updates

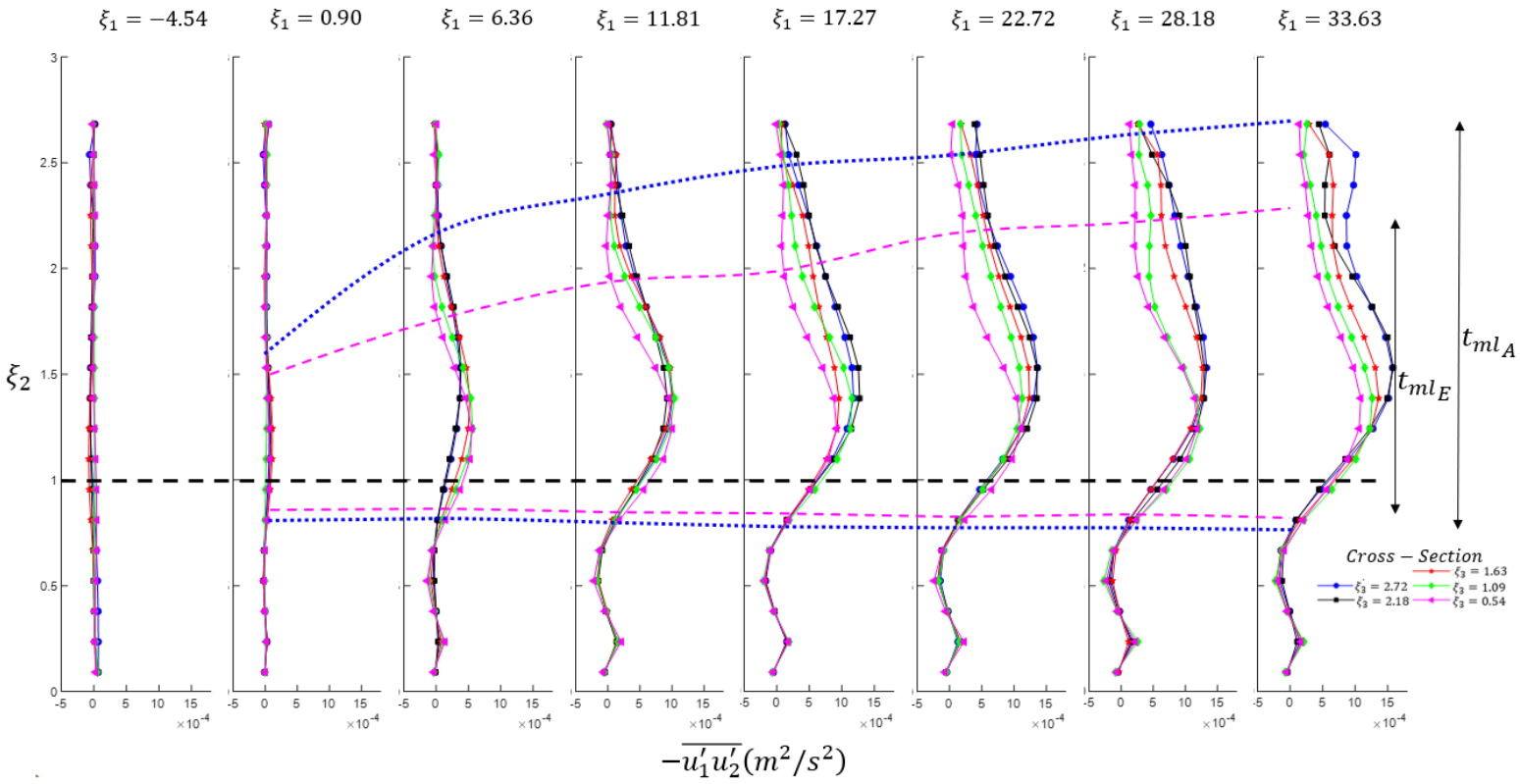


**Figure 12**. Reynolds stress profiles $-\overline{\boldsymbol{u_1' u_2'}}$. Where the blue and magenta dashed lines represent the longitudinal spatial variation of the thickness of the mixing layer in the center section $\boldsymbol{\xi_3 = 2.72}$ and near to the wall $\boldsymbol{\xi_3 = 0.54}$, respectively, and the black dashed line represents the top of the vegetation $\boldsymbol{\xi_2 = 1}$.

Tecnología y Ciencias del Agua

OPEN ACCESS

Check for updates

## Mixing layer

According to Raupach *et al*., Finnigan and Brunet (1996), and Ghisalberti & Nepf (2002), the velocity profile of a mixing layer can be analyzed with the following expression:

$$\frac{U_1-U_m}{\Delta U_1}=\frac{1}{2}\tanh\left(\frac{x_2-\bar{y}}{2\theta}\right) \quad (5)$$

For better understanding, Figure 1 shows the variables in the mixing layer. Where $U_m = U_1(y_r) + U_1(y_u)/2$, $\Delta U_1$ is the velocity difference for each cross section: $\Delta U_1 = U_1(y_r) - U_1(y_u)$, $U_1(y_r)$ and $U_1(y_u)$ indicate the velocity averaged at the upper and lower limit of the mixing layer respectively, $y_u$ and $y_r$ is the distance from the bottom of the channel to the value of the Reynolds stress with zero value below and above the maximum Reynolds stress value respectively, $\bar{y} = (y_r + y_u)/2$, this analysis is developed for each velocity profile in the longitudinal and cross-sectional sections. The momentum thickness $\theta$ is defined with the following expression:

$$\theta = \int_0^\infty \left[\frac{1}{4} - \left(\frac{U_1-U_m}{\Delta U_1}\right)^2\right] dx_2 \quad (6)$$

Figure 13 makes a comparison between the theoretical model to evaluate the hyperbolic tangent velocity profiles of a pure mixing layer and the experimental data.

Tecnología y Ciencias del Agua

OPEN ACCESS

Check for updates

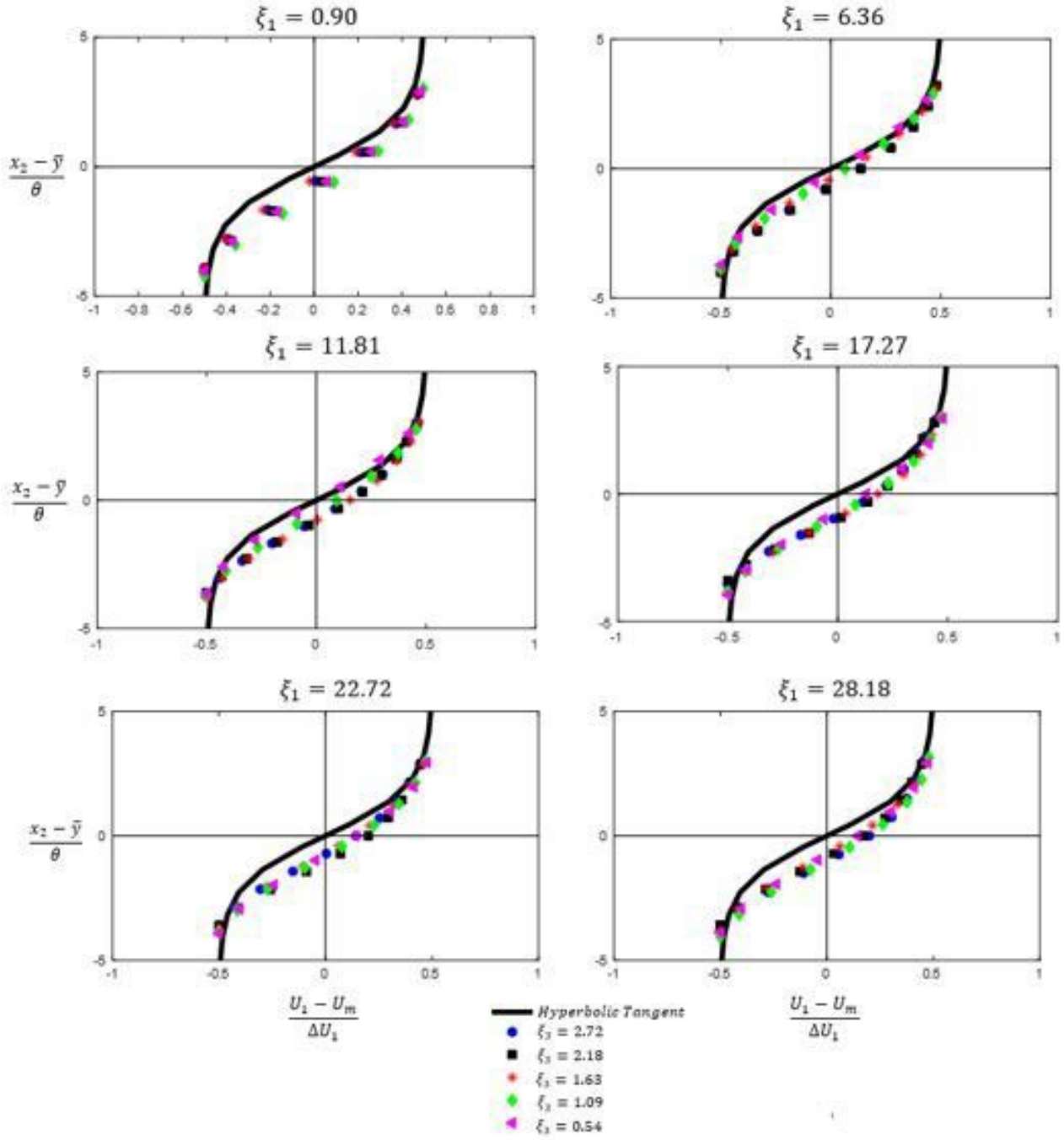

**Figure 13**. Comparison of the mean velocity profiles with the hyperbolic tangent profile of a mixing layer for each cross section for different positions in the longitudinal direction.

According to the results it is observed that the velocity profiles obtained in the experimentation resemble a mixing layer profile, therefore, it is concluded that a mixing layer is formed in an intermediate flow.

## Phenomenological model

To evaluate the evolution of the mixing layer longitudinally for each analysis section, it is proposed to apply a division of the flow field into four zones are described in Table 3 and shown in Figure 14.

**Table 3**. Division of the phenomenological model zones, where $\boldsymbol{X_i}$ is the beginning of analysis (zone upstream of the vegetation), $\boldsymbol{X_{FL}}$ is the beginning of the divergent zone, $\boldsymbol{X_{FD}}$ is the beginning of the development zone, $\boldsymbol{X_{ZD}}$ is the beginning of the fully developed zone, and $\boldsymbol{X_L}$ is the end of the field of analysis.

| Zone | Flow condition | Analysis space |
|---|---|---|
| **I** | Initial | $[X_i, X_{FL}]$ |
| **II** | Divergent | $[X_{FL}, X_{FD}]$ |
| **III** | Development | $[X_{FD}, X_{ZD}]$ |
| **IV** | Fully developed | $[X_{ZD}, X_L]$ |

Tecnología y Ciencias del Agua
OPEN ACCESS
Check for updates

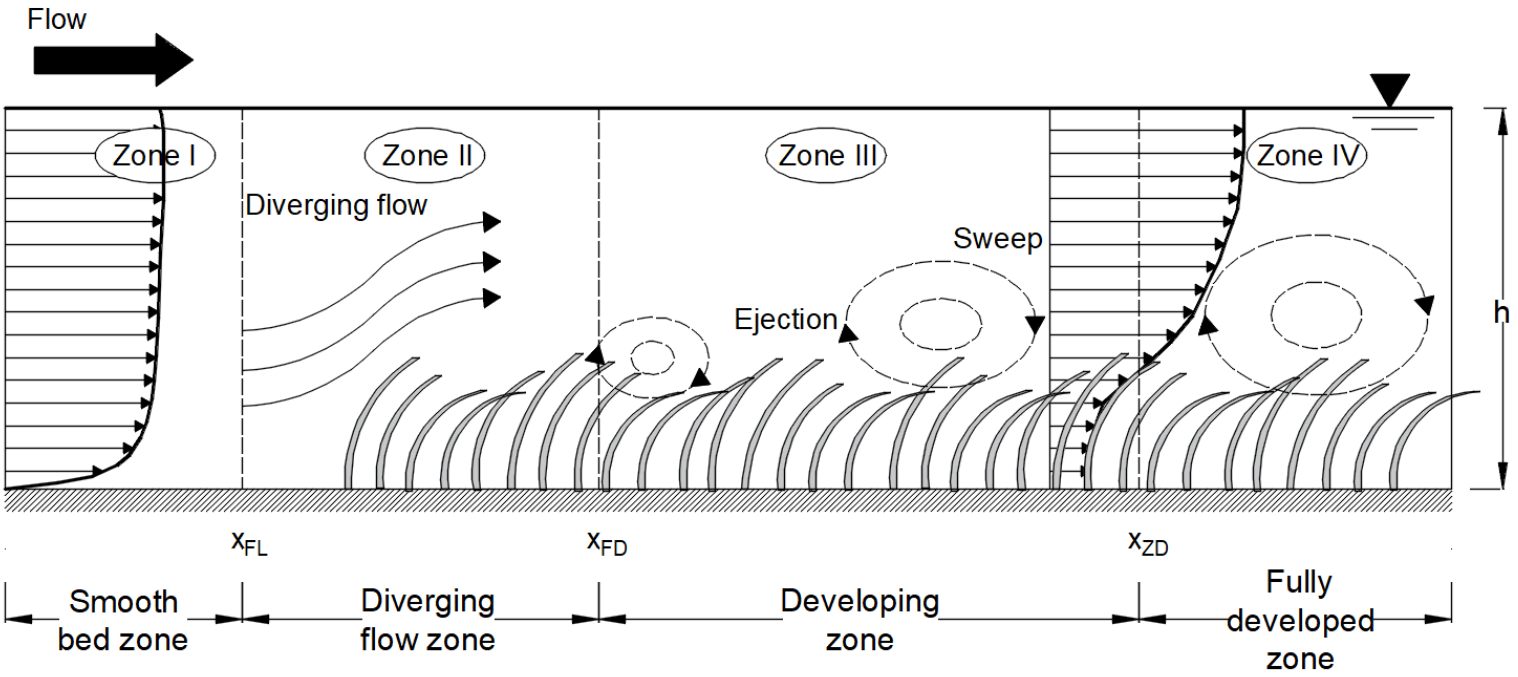


**Figure 14**. Phenomenological model of flow development through a zone of submerged vegetation (Okamoto & Nezu, 2013; Huai & Qian, 2015).

Upstream of the vegetation zone $(\xi_1 \leq X_{FL})$ the velocity profiles resemble a profile found in an open channel flow, since the vegetation does not affect the flow. At the beginning of the vegetation $(\xi_1 = 0)$ there is a high resistance to the flow and initiates an increase in the velocity above the vegetation and a deceleration within it. That is, part of the flow is diverted at the beginning of the vegetation zone. Zong & Nepf (2010)

call this phenomenon as divergent flow. The end of the divergent flow is denoted as $X_{FD}$.

Downstream the divergent flow zone ($\xi_1 \geq X_{FD}$), the velocity profiles have a high velocity gradient, as shown in Figure 1. This gradient creates an inflection point at $\xi_2 \approx 1$, inducing a Kelvin-Helmholtz instability, generating downstream vortices. The growth of these vortices is seen in the Reynolds stress profiles. This zone is defined as a development zone, the end of this is defined as $X_{ZD}$.

Downstream of the development zone ($\xi_1 \geq X_{ZD}$) the size of the vortices remains constant. This area is called a fully developed zone.

Figure 15 shows the effect of vegetation on the main velocity averaged vertically $U_{1_m}$ in the zone without and with vegetation. To determine this averaged velocity, the following expression is used:

$$U_{i_m} = \frac{1}{h}\int_0^{\zeta=h} U_i\,(\xi_1, \zeta, \xi_3 = cte)d\zeta \qquad (7)$$

Tecnología y Ciencias del Agua
OPEN ACCESS
Check for updates

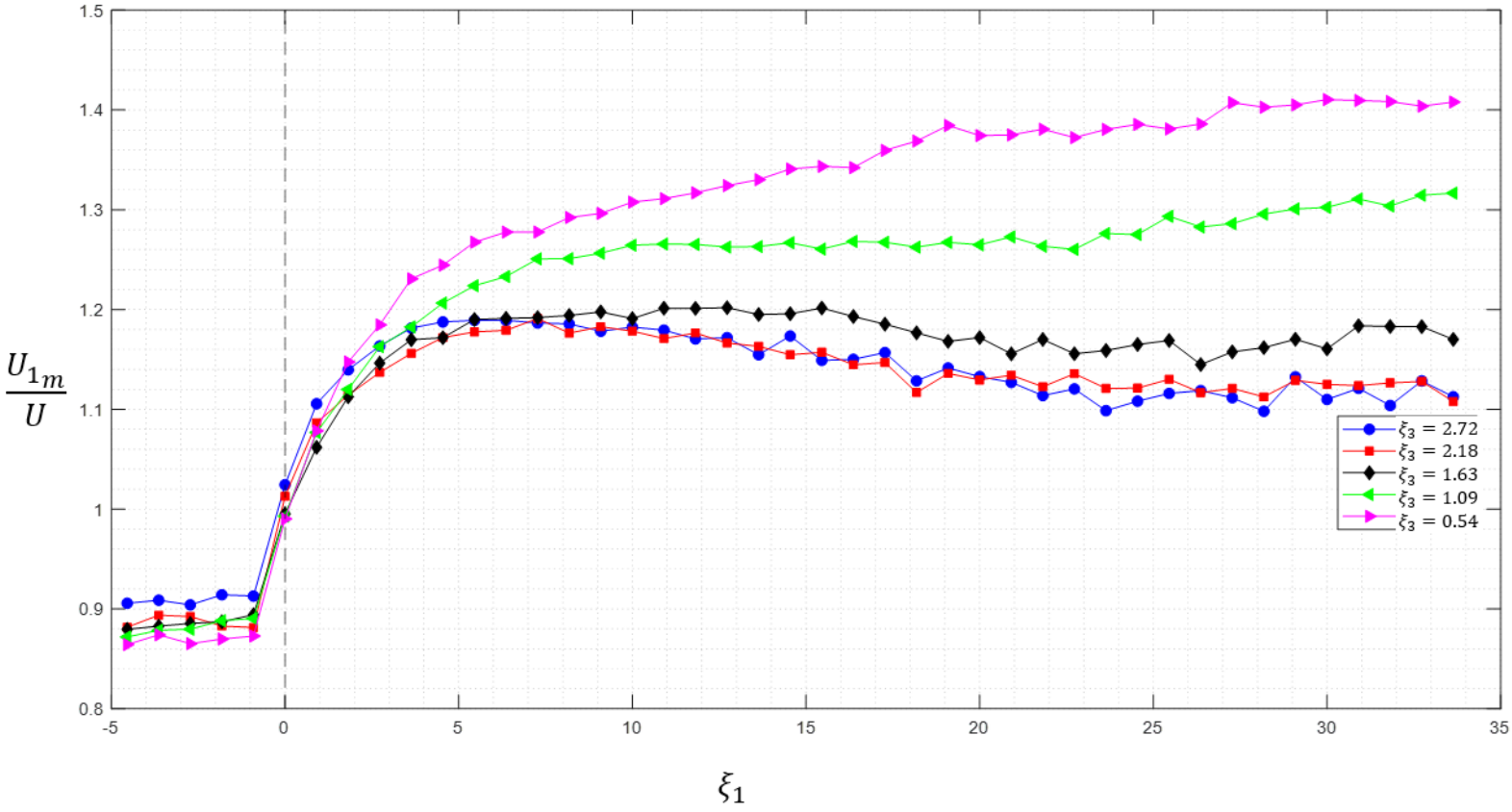


**Figure 15**. Variation of the mean velocity in the main direction, upstream and over vegetation.

Observing in the zone upstream of vegetation, $-5 \leq \xi_1 \leq 0$, there is a velocity with little variability, $\partial U_{1_m}/\partial x \approx 0$. For the central zone of the channel $\xi_3 = 1.63, 2.18, 2.72$, the flow velocity increases to a maximum value in a range $0 \leq \xi_1 \leq 5$, downstream this maximum value the velocity decreases, because the mixing layer reaches the free surface, as shown in Figure 11, being a zone of high turbulence. However, for the zone near

to the wall $\xi_3 = 0.54, 1.09$, the increase in velocity remains constant, because the mixing layer does not reach the free surface, therefore, the turbulence zone is smaller and the deceleration of the flow is not generated, see Figure 11.

The starting point of the divergent flow, $X_{FL}$, and the length of the Divergent Zone (Zone II), $L_{FD} = X_{FD} - X_{FL}$, is determined from the vertical velocity averaged in the vertical, $U_{2_m}$. Applying equation (7) evaluates the divergent flow, as shown in Figure 16. Observing a rapid increase in vertical velocity in $-2.73 \leq \xi_1 \leq 0$, where the maximum value is at the beginning of the vegetation zone $(\xi_1 = 0)$ for each section. The start of the divergent flow, $X_{FL}$, is determined when the vertical velocity increases, that is, when $dU_{2_m}/dx_1 > 0$, therefore, for the five sections $X_{FL} = -2.73$. However, the start of the development zone, $X_{FD}$, for each section varies as it approaches the wall. $X_{FD}$ is obtained up to the point where the vertical velocity approaches zero, $U_{2_m} \approx 0$, as shown in Figure 16. Then Table 4 shows the length of Zone II, $L_{FD}$.

Tecnología y Ciencias del Agua
OPEN ACCESS
Check for updates

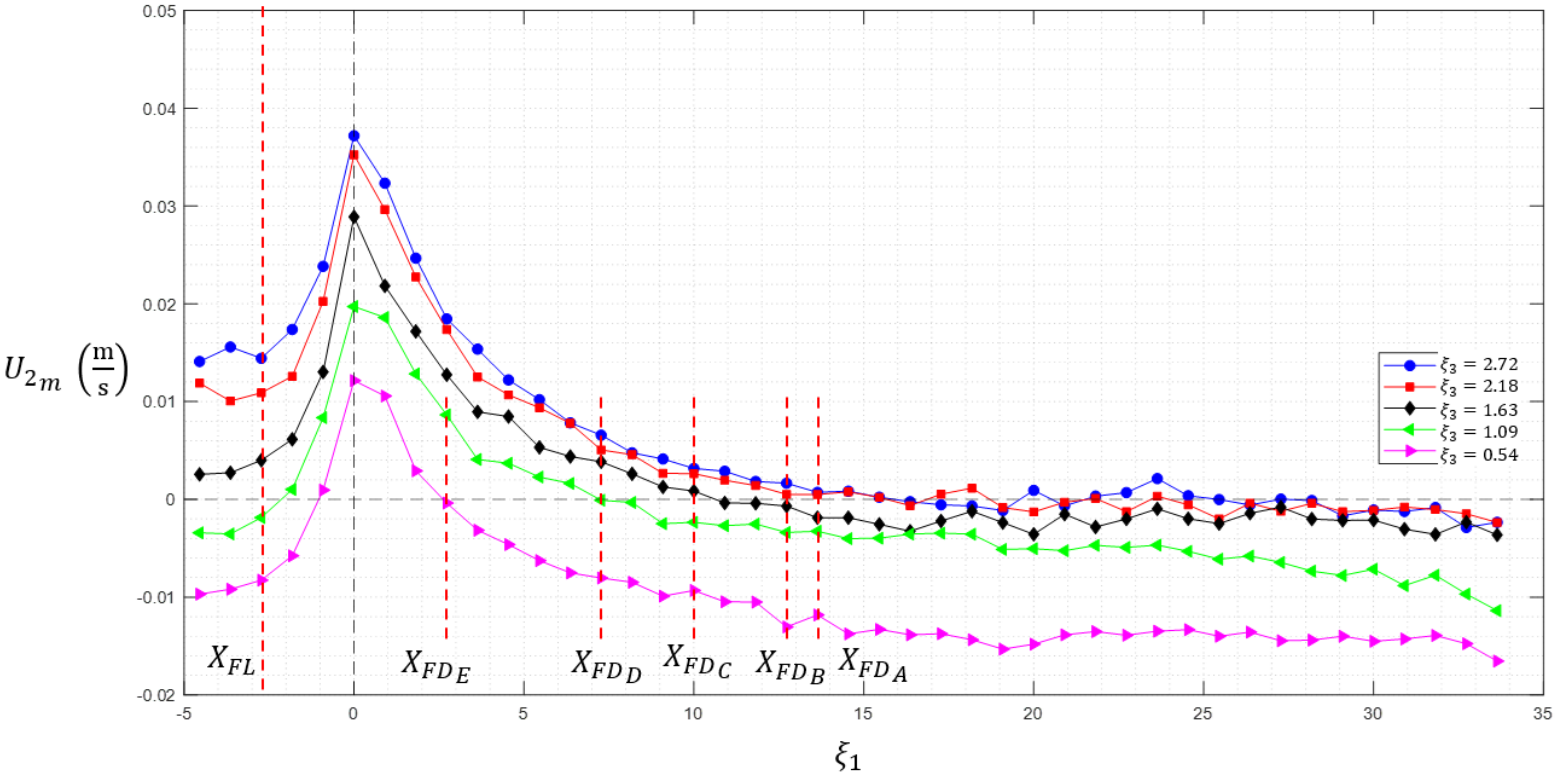


**Figure 16**. Variation of the average velocity vertically for each section.

**Table 4**. Divergent flow length, $L_{FD}$.

| Zone\$\xi_3$ | 2.72 | 2.18 | 1.63 | 1.09 | 0.54 |
|---|---|---|---|---|---|
| $X_{FL}$ | −2.73 | −2.73 | −2.73 | −2.73 | −2.73 |
| $X_{FD}$ | 13.63 | 12.72 | 10 | 7.27 | 2.72 |
| $L_{FD}$ | 16.36 | 15.45 | 12.73 | 10 | 5.45 |

To better visualize the Diverging Flow Zone, Figure 17 shows the zone with the highest vertical velocity $U_2$.

Tecnología y Ciencias del Agua
OPEN ACCESS
Check for updates

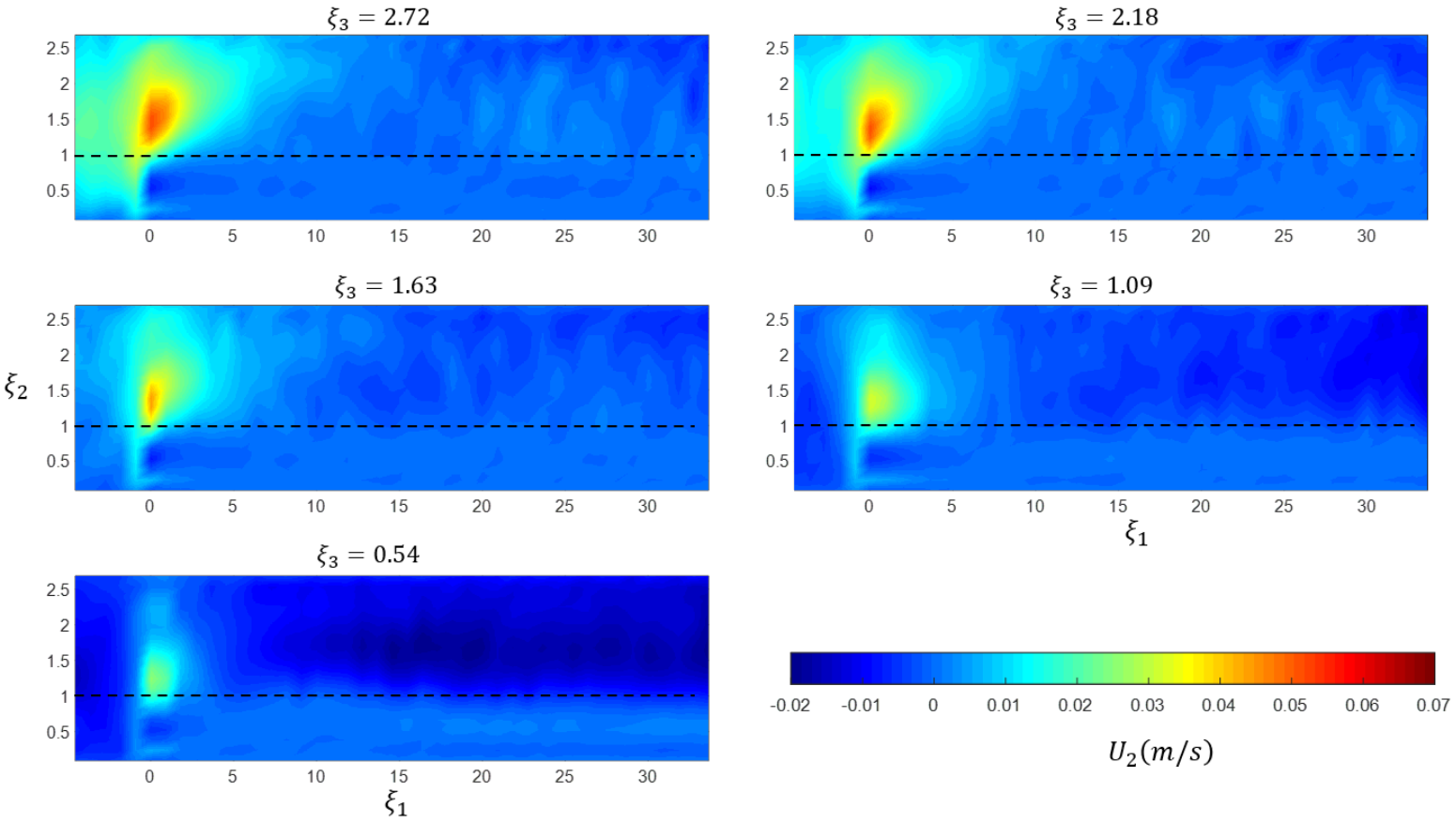


**Figure 17**. Contours of mean velocity in the vertical direction $\boldsymbol{U_2}$. Where the dashed line represents the top of the vegetation $\boldsymbol{\xi_2 = 1}$.

Downstream of the divergent flow zone the velocities vertically become small, observing negative velocity values, $U_2 < 0$. Then for $\xi_2 \geq X_{FD}$ the mixing layer it grows gradually until the size of the mixing layer, $t_{ml}$, remains constant, that is, when $dt_{ml}/dx_1 \approx 0$, is located in the start of

the fully developed zone, $X_{ZD}$. Figure 12 shows the spatial variation of the mixing layer. Then for each section, $X_{ZD}$ is obtained with the spatial variation of the size of the mixing layer, as shown in Figure 18.

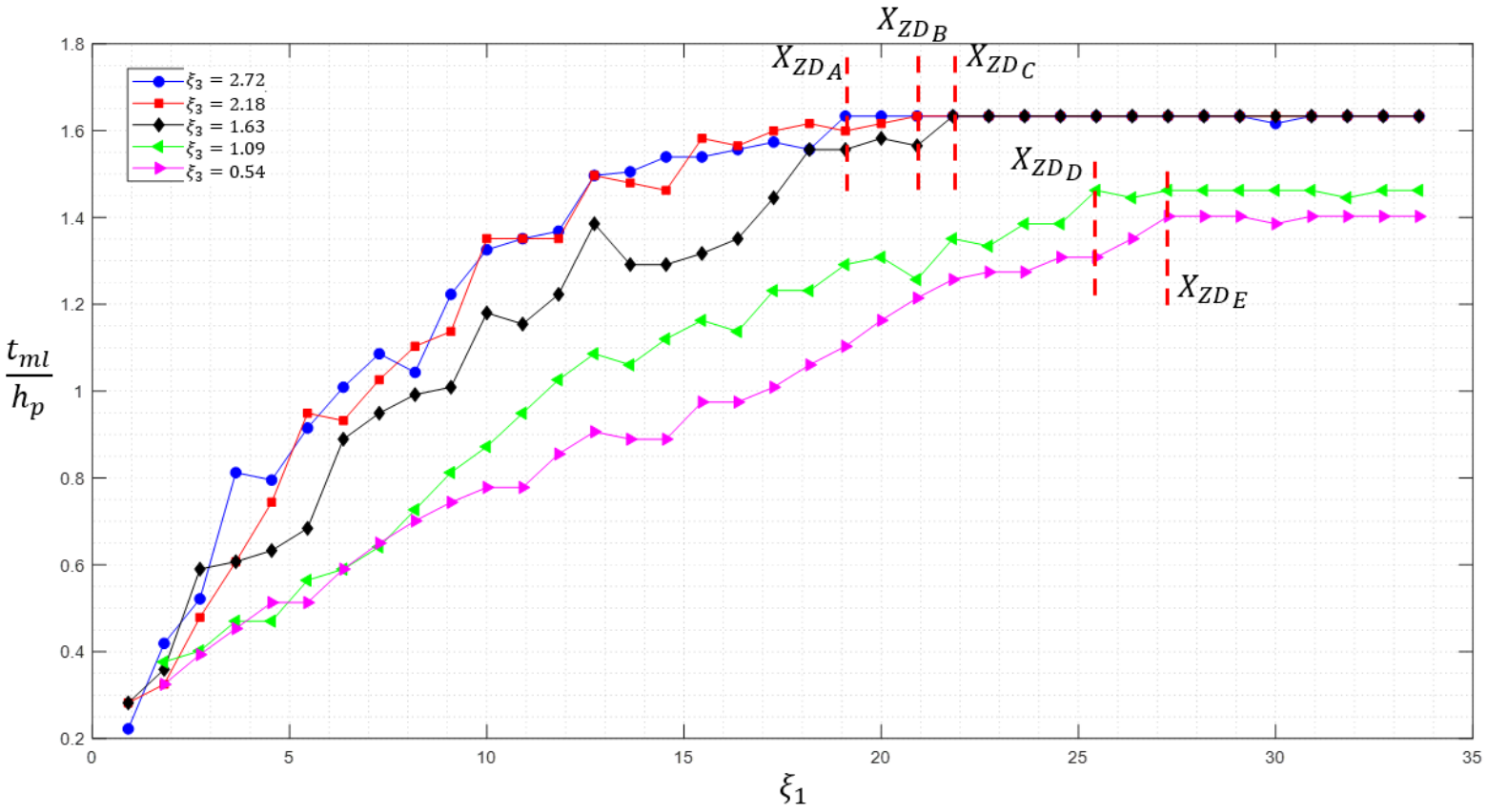


**Figure 18**. Spatial variation of the mixing layer thickness, $t_{ml}$, for each section.

Tecnología y Ciencias del Agua

OPEN ACCESS

Check for updates

For comparison, Figure 19 shows the variation of momentum thickness, $\theta$, which is a measure of growth of the shear layer. Noting that $t_{ml}$ and $\theta$ grow rapidly downstream from the start of the vegetation zone.

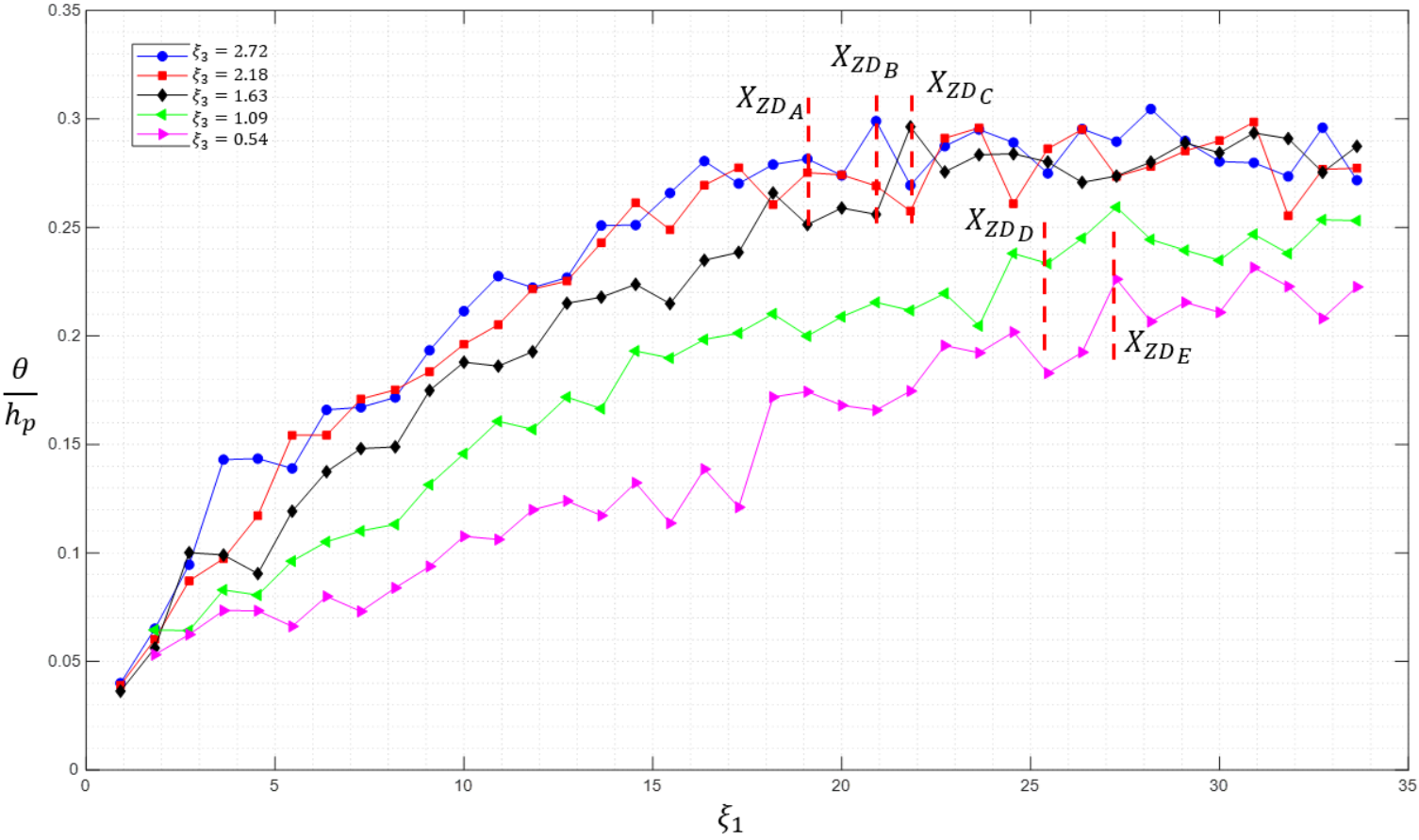


**Figure 19**. Spatial variation of the momentum thickness, $\theta$, for each section.

Then the length of the Development Zone is obtained with $L_{ZD} = X_{ZD} - X_{FD}$. Table 5 shows the Zone III lengths for each section.

**Table 5**. Length of development zone, $\boldsymbol{L_{ZD}}$.

| **Zone\$\xi_3$** | **2.72** | **2.18** | **1.63** | **1.09** | **0.54** |
|---|---|---|---|---|---|
| $\boldsymbol{X_{FD}}$ | 13.63 | 12.72 | 10 | 7.27 | 2.72 |
| $\boldsymbol{X_{ZD}}$ | 19.09 | 20.91 | 21.82 | 25.45 | 27.27 |
| $\boldsymbol{L_{ZD}}$ | 5.45 | 8.19 | 11.82 | 18.18 | 24.55 |

Finally, downstream of Zone III, $\xi_1 \geq X_{ZD}$, is the Fully Developed Zone (Zone IV), $L_{CD}$, to where the vegetation zone ends. Figure 20 shows the phenomenological model of flow development for this test, which shows the variations of the four zones in the transverse direction, $x_3$.

Tecnología y Ciencias del Agua

OPEN ACCESS

Check for updates

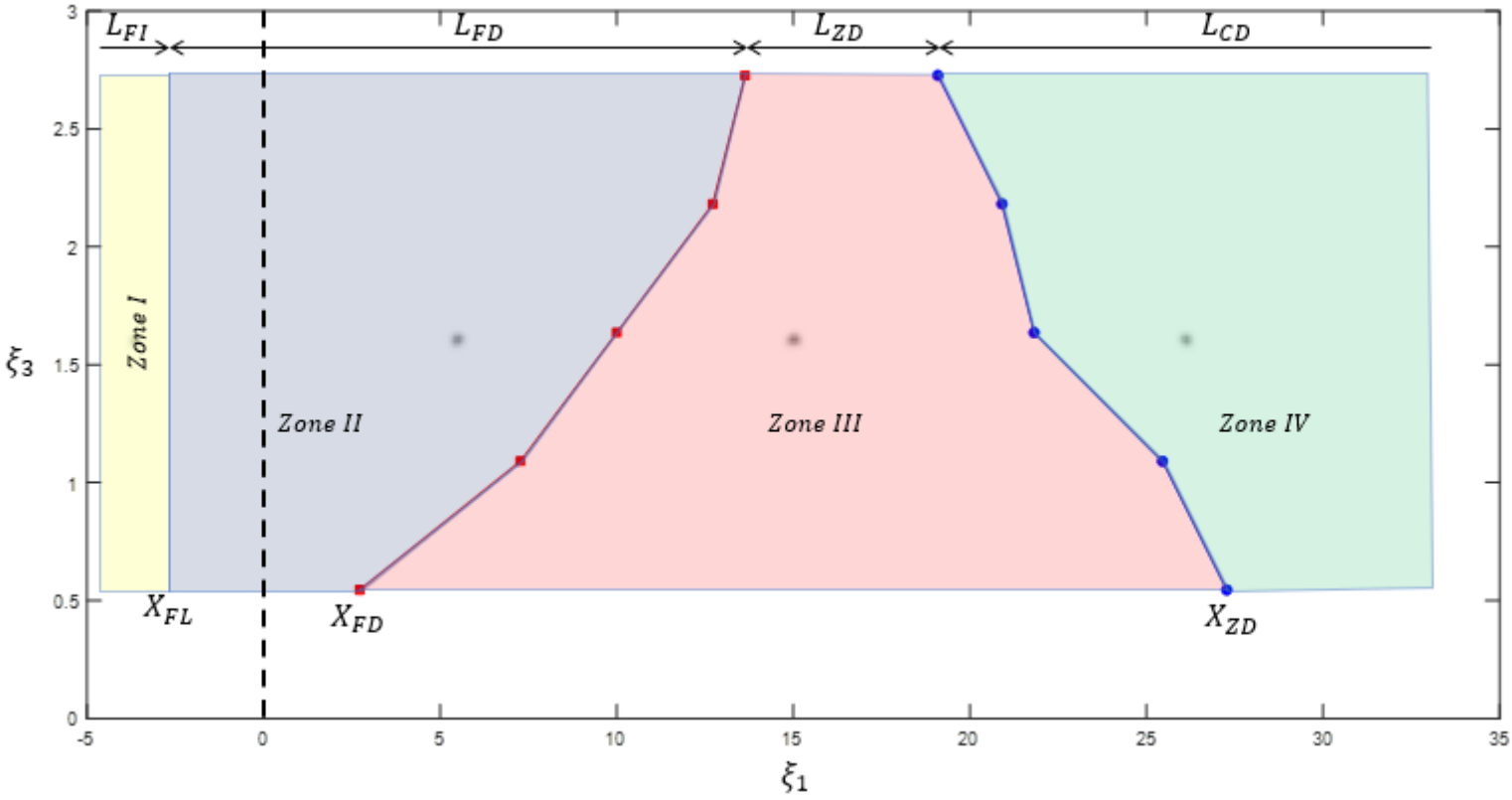


**Figure 20**. Phenomenological model. Where the black dashed line indicates the start of the vegetation zone, $\boldsymbol{\xi_1 = 0}$.

It is observed that the length of Zone III, $L_{ZD}$, for the center of the channel, $\xi_3 = 2.72$, is less than the zone near to the wall, $\xi_3 = 0.54$. This indicates that in the center of the channel there is a greater resistance, since in the center there is a deceleration of the flow is high compared to the zone near to the wall, this is observed in Figure 15.

Tecnología y Ciencias del Agua

OPEN ACCESS

Check for updates

## Quadrant analysis

A quadrant analysis was performed for instantaneous Reynolds stress $-u_1'(t)u_2'(t)$ for the analysis of turbulent structures that contribute to momentum transport. The basic principle of quadrant analysis is to decompose Reynolds stresses into four types of flows, called $Q_1$, $Q_2$, $Q_3$and $Q_4$ into the plane $u_1' - u_2'$ as a function of the signs of fluctuation of the main $u_1'$ and vertical $u_2'$ velocity as shown in Figure 21.

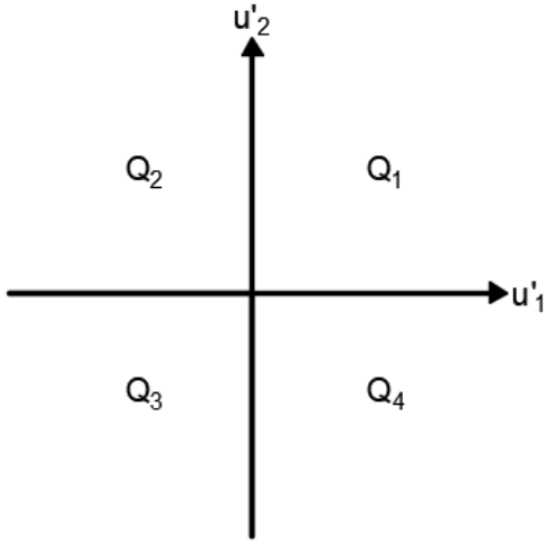


**Figure 21**. Quadrant diagram $\boldsymbol{u_1' - u_2'}$.

Reynolds stress quadrant $RS_i$ is defined as follows (Okamoto *et al*., 2012; Okamoto & Nezu, 2013):

$$RS_i = \lim_{T\to\infty} \frac{1}{T} \int_0^T (u_1' u_2') I_i \, dt \qquad (8)$$

Where $T$ is the duration of the measurement. If $(u_1', u_2')$ exist in quadrant $Q_i$, then $I_i = 1$, otherwise $I_i = 0$.

Each quadrant $(u_1', u_2')$ corresponds to the following coherent events:

$Q_1\ (u_1' > 0\ , u_2' > 0)$ : External interaction, which is the upward movement of the high-speed flow.

$Q_2\ (u_1' < 0\ , u_2' > 0)$ : Ejection, which is the upward movement of the low-speed flow.

$Q_3\ (u_1' > 0\ , u_2' < 0)$ : Internal interaction, which is the downward movement of the low-speed flow.

$Q_4\ (u_1' < 0\ , u_2' < 0)$ : Sweep, which is the downward movement of the high-speed flow.

Figure 22 shows the vertical distribution of the Reynolds stress quadrants, $RS_i$, for the four zones of the phenomenological model in $\xi_3 = 2.72$. In addition, the plane of the fluctuating velocities $(u_1' - u_2')$ for $\xi_2 = 1.2$, where they indicate the percentage of contribution of each quadrant. In the initial flow zone, $\xi_1 = -2.72$, it is observed that the values are small and the percentage of contribution of turbulent structures to the momentum transport is similar, that is, no organized structures are observed.

Tecnología y Ciencias del Agua

OPEN ACCESS

Check for updates

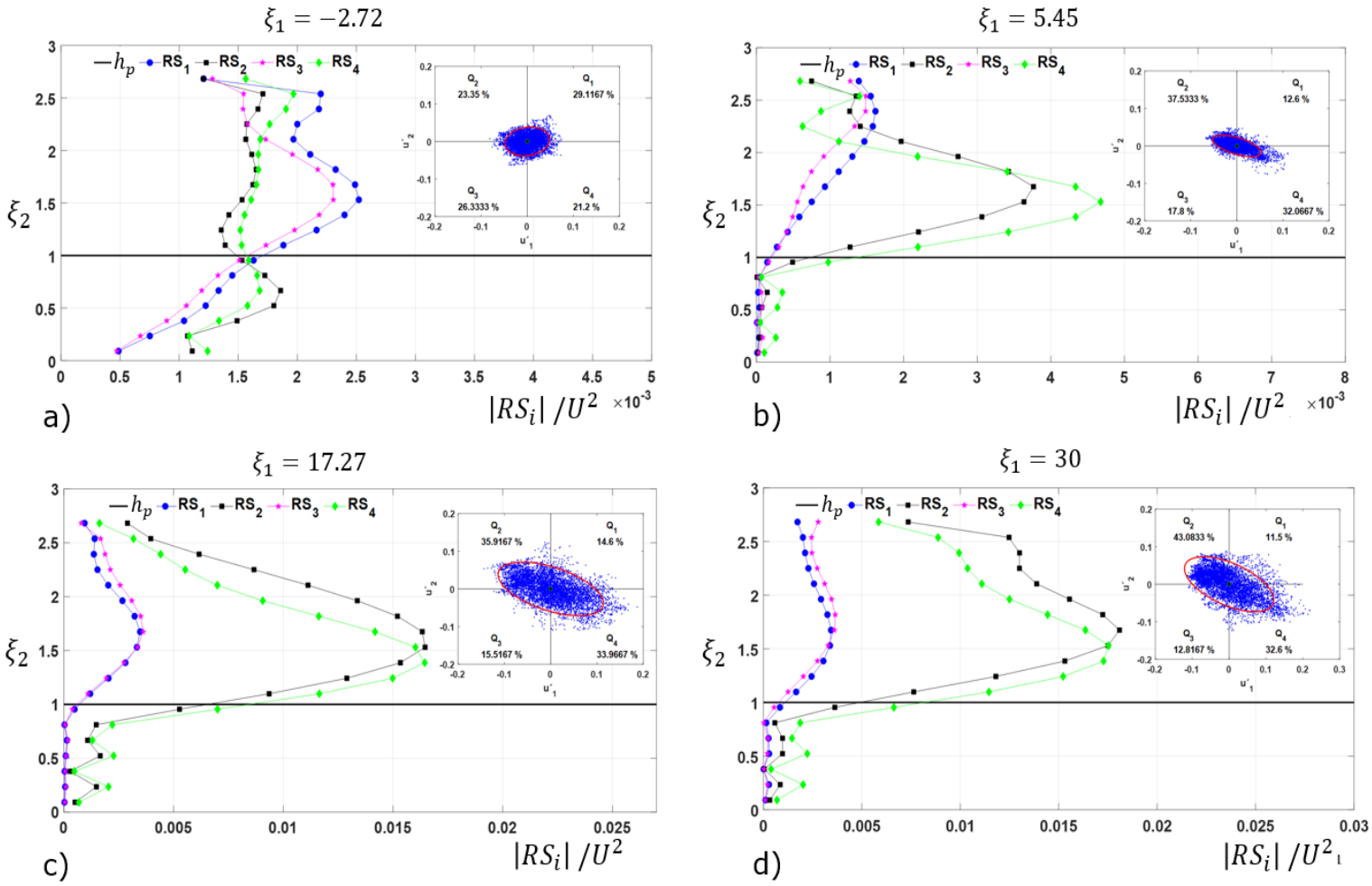


**Figure 22**. Reynolds stress quadrants for the central section of the channel $\xi_3 = 2.72$. a) initial zone ($\xi_1 = -2.72$); b) divergent zone ($\xi_1 = 5.45$); c) developed area ($\xi_1 = 17.27$); d) fully developed zone ($\xi_1 = 30$).

In the Divergent Flow Zone, $\xi_1 = 5.45$, over the vegetation zone $(\xi_2 \geq 1)$, it is observed that the dominant structure is the sweep, $RS_4$, see Figure 22.b.

In the Development zone, $\xi_1 = 17.27$, the dominant structures are the expulsion and sweep by effect of the vortices in the mixing layer, which are the low-speed upward and high-speed downward movements respectively Huai *et al.* (2019). This is observed in $\xi_2 \approx 1.5$, where the maximum value of Reynolds stresses is found (Figure 22c).

In the Fully Developed Flow zone, $\xi_1 = 30$, the ejection and sweep structure increase approximately $11\,\%$ with respect to the Development zone. These results indicate that the contribution of momentum transport between the vegetation zone and the zone above it is mainly due to the conditions of expulsion and sweeping.

To visualize the turbulent structures throughout the flow region, Figure 23 shows the contours of the Reynolds stress quadrants for all sections. It is observed that for all sections the structures that contribute most to the transport of momentum is the structure of ejection and sweep. In addition, it is observed that the maximum values are in the mixing layer zone.

Tecnología y Ciencias del Agua

OPEN ACCESS

Check for updates

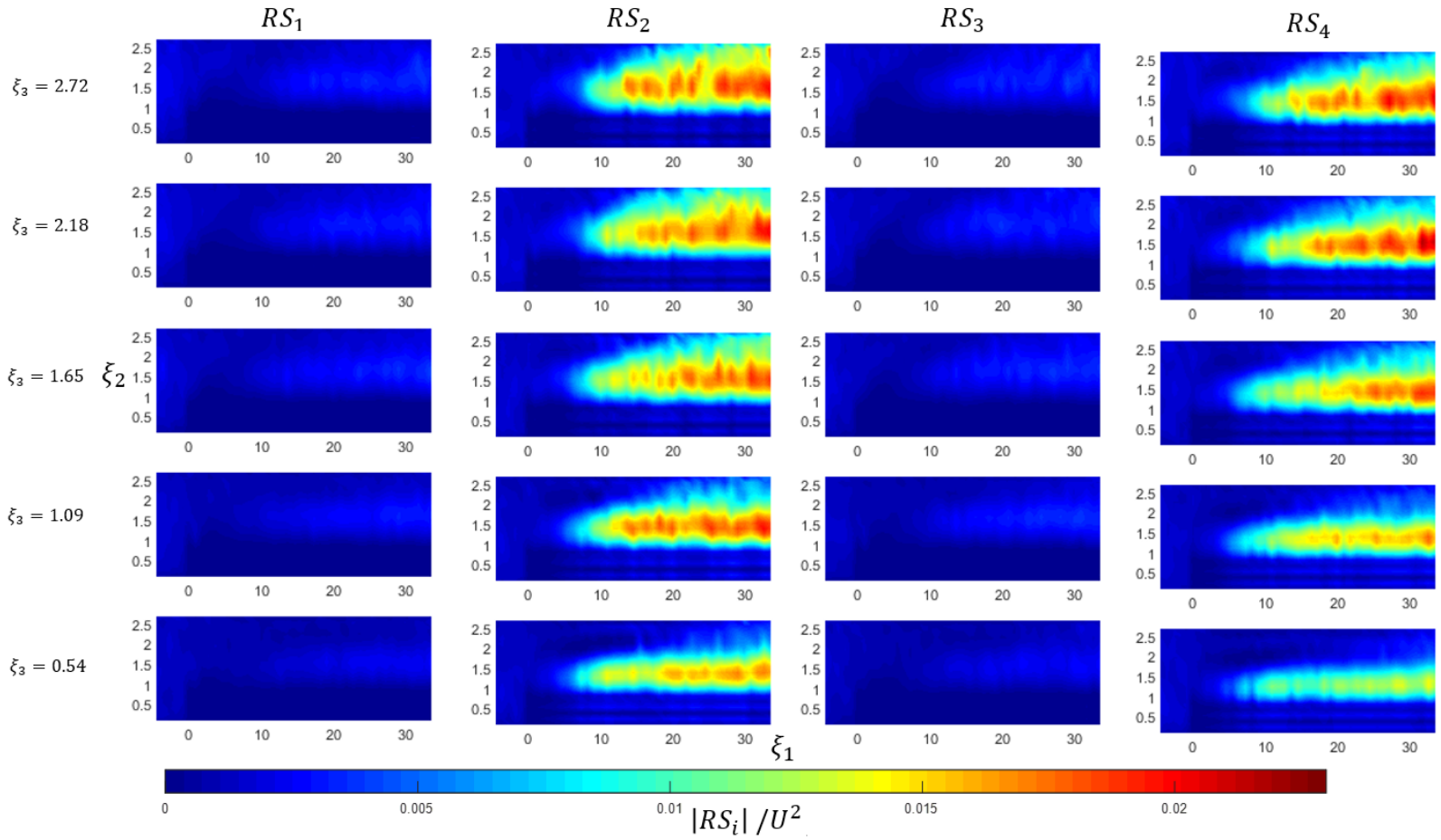


**Figure 23**. Contours of the Reynolds stress quadrants, $\boldsymbol{RS_i}$, for each cross section $\boldsymbol{\xi_3}$, evaluated over space $\boldsymbol{x_1 - x_2}$.

Once the turbulent structures with the greatest contribution have been found, Figure 24 compares the contributions of the sweep and ejection movement, using the Equation (9):

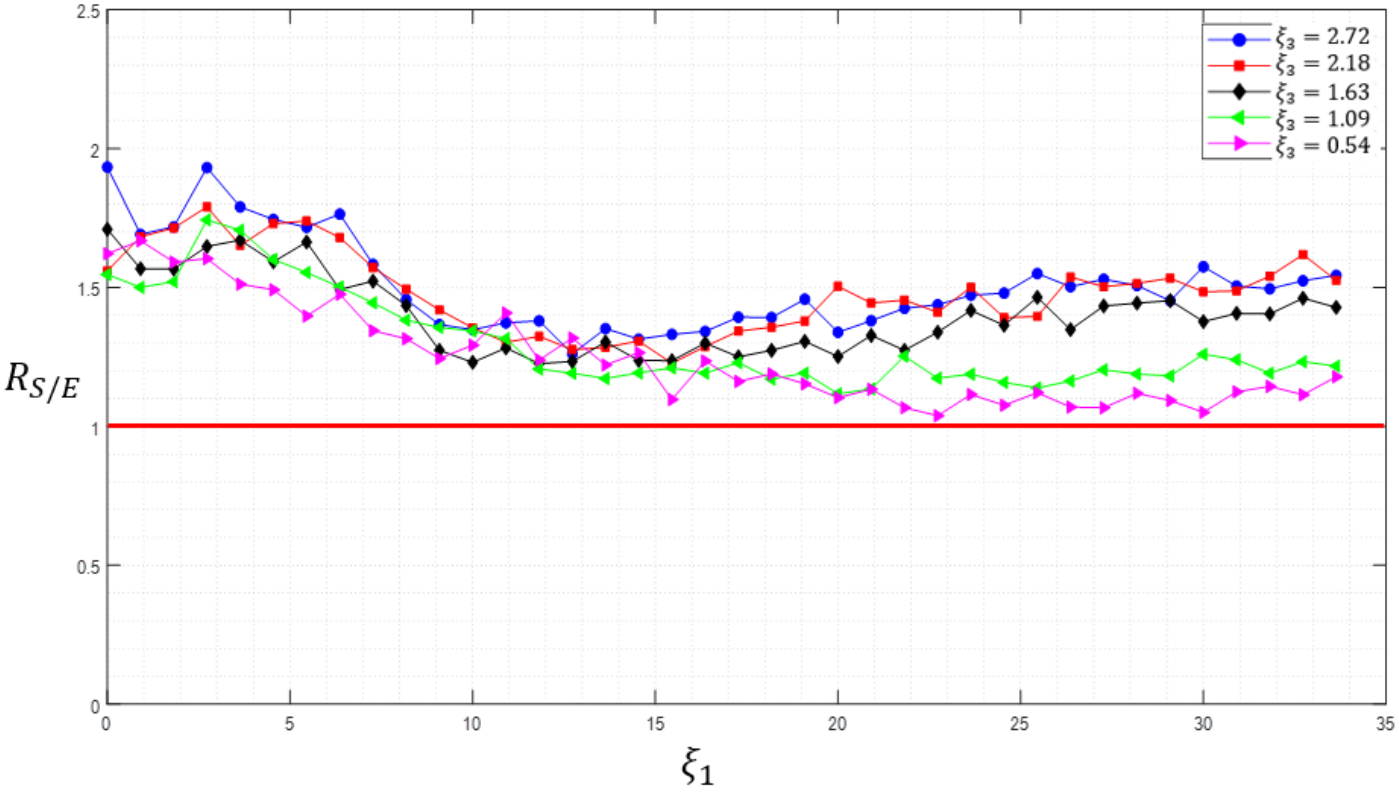


**Figure 24**. Relationship between sweep and ejection structures.

$$R_{S/E} = \frac{1}{h}\int_0^{\zeta=h} \frac{RS_4}{RS_2} d\zeta \qquad (9)$$

Applying Equation (9) for each section we obtain the relations between sweep and ejection $R_{S/E}$, observing a relationship $R_{S/E} > 1$ for all cross sections, therefore, the structure with the greatest contribution to vertical momentum transport is due to sweep motion.

Tecnología y Ciencias del Agua

OPEN ACCESS

Check for updates

# Conclusions

In this study, turbulence measurements were performed in a channel with a patch of vegetation of finite length to examine the creation and evolution downstream of turbulent structures in the mixing layer above vegetation.

The mean velocity profiles confirm the presence of an inflection point caused by Kelvin-Helmholtz type instability similar to theoretical analysis when two potential flows of different velocity are presented. By vertically distributing Reynolds stresses, the mixing layer was identified, as well as the variation in size along the vegetation patch and transverse direction. Noting that the size of the mixing layer stops growing in the Fully Developed Zone ($x_1 \geq X_{ZD}$), because the mixing layer extends to the free surface. In addition, the size of the mixing layer for $\xi_3 = 2.72$ (section $A$) is approximately $20\,\%$ larger compared to $\xi_3 = 0.54$ (section $E$), this is clearly seen in the contours of Reynolds stresses, see Figure 11 because the high-speed flow field is larger than the low-speed, as shown in Figure 9.

With the phenomenological model of the flow, the four zones of the flow were identified for the five analysis sections, obtaining the lengths of

these zones for the sections, as shown in Figure 20. Looking for $\xi_3 = 0.54$ (section $E$) requires a greater distance for the mixing layer to fully develop compared to $\xi_3 = 2.72$ (section $A$). This is visualized in the magnitude of Reynolds stresses.

A quadrant analysis was applied to identify the turbulent structures that contribute to the momentum transport, it is visualized that for the Initial Flow Zone an organized structure is not observed. In the Development and Fully Developed Zone, ejection and sweep structures appear near the top of the vegetation. These results indicate that the contribution of momentum transport between the vegetation zone and the zone above it is mainly due to the ejection and sweep structures.

With the methodology used in this paper it is possible to identify the presence of a mixing layer and the characteristics of the turbulent structures present in it. In addition, with the use of a phenomenological model applied to several sections, a map was generated that shows the variation of the four zones along a channel with vegetation, which can be used for channels with vegetation with characteristics similar to those used in this experiment, such as the submergence ratio, flexural rigidity, dimensionless density and the main mean velocity.

## Acknowledgment

The authors thank Dr. Jorge Armando Laurel Castillo for conducting a previous review of this work. To the National Council of Science and

Technology (CONACYT), the National Autonomous University of Mexico (UNAM) and the Mexican Institute of Water Technology (IMTA).

## References

Carollo, F. G., Ferro, V., & Termini, D. (2005). Flow resistance law in channels with flexible submerged vegetation. *Journal of Hydraulic Engineering*, 554-564.

Finnigan, J. (2000). Turbulence in plant canopies. *Annual Reviews Fluid Mechanics*, 519-571.

Ghani, U., Ali, S., & Latif, A. (October, 2013). Impact of vegetation density on flow characteristics in a straight compound channel. *Journal of Engineering & Technology*, 32(4), 631-638.

Ghisalberti, M., & Nepf, H. M. (2002). Mixing layers and coherent structures in vegetated aquatic flows. *Journal of Geophysical Research*, 107(C2), 1-11. DOI: 10.1029/2001JC000871

Ho, C.-M., & Huerre, P. (1984). Perturbed free shear layers. *Annual Review of Fluid Mechanics*, 16, 365-424.

Huai, W.-X., & Qian, Z.-D. (2015). Large-eddy simulation of turbulent rectangular open-channel flow with an emergent rigid vegetation patch. *Advances in Water Resources*, 80, 30-42. Recovered from https://doi.org/10.1016/j.advwatres.2015.03.006

Huai, W.-X., Zhang, J., Wang, W.-J., Katul, G. G., Tang, X., & Cheng, Y.-G. (2019). The structure of turbulent flow through submerged flexible vegetation. *Journal of Hydrodynamics*, 31, 274-292.

Järvelä, J. (2004). Determination of flow resistance caused by non-submerged woody vegetation. *International Journal of River Basin Managment*, 2(1), 61-70. DOI: 10.1080/15715124.2004.9635222

Jeon, H.-S. (2015). *Flow and sediment-POM transport in strean with vegetation.* Nagoya, Japan: Nagoya University.

Kouwen, N., & Li, R.-M. (1980). Biomechanics of vegetative channel linings. *Journal of the Hydraulics Division*, 106, 1085-1103.

Maltese, A., Cox, E., Folkard, A. M., Ciraolo, G., Loggia, G., & Lambardo, G. (2007). Laboratory measurements of flow and turbulence in discontinous distributions of ligulate seagrass. *Journal of Hydraulic Engineering*, 133(7), 750-760.

Nepf, H., & Vivoni, E. (2000). Flow structure in depth-limited, vegetated flow. *Journal of Geophysical Research*, 105(28), 28.547-28.557. Recovered from https://doi.org/10.1029/2000JC900145

Nezu, I., & Sanjou, M. (2008). Turbulence structure and coherent motion in vegetated canopy open-channel flows. *Journal of Hydro-Environment Research*, 2(2), 62-90. DOI: 10.1016/j.jher.2008.05.003

Nikora, V., Larned, S., Nikora, N., Debnath, K., Cooper, G., & Reid, M. (2008). Hydraulic resistance due to aquatic vegetation in small streams: Field study. *Journal of Hydraulic Engineering*, 134(9), 1326-1332.

Okamoto, T.-A., & Nezu, I. (2009). Turbulence structure and "Monami" phenomena in flexible vegetated open-channel flows. *Journal of*

*Hydraulic Engineering*, 47(6), 798-810. Recovered from https://doi.org/10.3826/jhr.2009.3536

Okamoto, T.-A., & Nezu, I. (2010). Flow resistance law in open-channel flows with rigid and flexible vegetation. *River Flow*, 261-268. Recovered from https://izw.baw.de/e-medien/river-flow-2010/PDF/A2/A2_03.pdf

Okamoto, T.-A., & Nezu, I. (2013). Spatial evolution of coherent motions in finite-length vegetation patch flow. *Environmental Fluid Mechanics*, 13(5), 417-434. DOI: 10.1007/s10652-013-9275-6

Okamoto, T.-A., Nezu, I., & Ikeda, H. (2012). Vertical mass and *momentum* transport in open-channel flows with submerged vegetations. *Journal of Hydro-Environment Research*, 6(4), 287-297. DOI: 10.1016/j.jher.2012.03.002

Palmer, V. (1945). A method for designing vegetated waterways. *Agricultural Engineering*, 26(12), 516-520.

Poggi, D., Porporato, A., & Ridolfi, L. (2004). The effect of vegetation density on canopy sub-layer turbulence. *Boundary-Layer Meteorology*, 111, 565-587.

Raupach, M. R., Finnigan, J. J., & Brunet, Y. (1996). Coherent eddies and turbulence in vegetation canopies: The mixing-layer analogy. *Boundary-Layer Meteorology*, 78, 351-382.

Sukhodolov , A., & Sukhodolova, T. (2006). Evolution of mixing layers in turbulent flow over submerged vegetation: Field experiments and measurement study. *Proceedings of the International Conference*

*on Fluvial Hydraulics River Flow 2006* September 6–8, 2006 Lisbon, Portugal, Taylor and Francis, London, v. 1: 525–534. Vargas-Luna, A., Crosato, A., & Uijttewaal, W. S. (2015). Effects of vegetation on flow and sediment transport: Comparative analyses and validation of predicting models. *Earth Surface Processes and Landforms*, 157-176. Recovered from https://doi.org/10.1002/esp.3633

Wilson, C. (2007). Flow resistance models for flexible submerged vegetation. *Journal of Hydrology*, 342(3-4), 213-222.

Wilson, C. A., Stoesser, T., Bates, P. D., & Btemann-Pinzen, A. (2003). Open channel flow through different forms of submerged flexible vegetation. *Journal of Hydraulic Engineering*, 129(11), 847-853.

Zong , L., & Nepf, H. (2010). Flow and deposition in and around a fi nite patch of vegetation. *Geomorphology*, 116(3-4), 363-372. Recovered from https://doi.org/10.1016/j.geomorph.2009.11.020